UNIVERSIDADE FEDERAL DO RIO GRANDE DO SUL
INSTITUTO DE PESQUISAS HIDRÁULICAS
PROGRAMA DE PÓS-GRADUAÇÃO EM RECURSOS HÍDRICOS E SANEAMENTO AMBIENTAL

ANA PAULA DALCIN

ADAPTATION PATHWAYS TO RECONCILE HYDROPOWER GENERATION AND AQUATIC ECOSYSTEMS RESTORATION

PORTO ALEGRE
2023

ANA PAULA DALCIN

SOLUÇÕES PARA CONCILIAÇÃO DA GERAÇÃO HIDRELÉTRICA E RECUPERAÇÃO DE ECOSSISTEMAS AQUÁTICOS

Tese de doutorado apresentada ao Programa de Pós-graduação em Recursos Hídricos e Saneamento Ambiental da Universidade Federal do Rio Grande do Sul, como requisito parcial à obtenção do grau de doutor.

Orientador: Prof. Dr. Guilherme Fernandes Marques
Coorientador: Prof. Dr. Amaury Tilmant

PORTO ALEGRE

2023

Dalcin, Ana Paula
Adaptation Pathways to Reconcile Hydropower Generation and Aquatic Ecosystem Restoration / Ana Paula Dalcin. -- 2023.
155 f.
Orientadora: Guilherme Fernandes Marques.

Coorientadora: Amaury Tilmant.

Tese (Doutorado) -- Universidade Federal do Rio Grande do Sul, Instituto de Pesquisas Hidráulicas, Programa de Pós-Graduação em Recursos Hídricos e Saneamento Ambiental, Porto Alegre, BR-RS, 2023.

1. vazões ambientais. 2. planejamento de sistemas hidrelétricos. 3. gestão de recursos hídricos. 4. recuperação de ecossistemas. 5. otimização multiobjetivo. I. Marques, Guilherme Fernandes, orient. II. Tilmant, Amaury, coorient. III. Título.

ANA PAULA DALCIN

ADAPTATION PATHWAYS TO RECONCILE HYDROPOWER GENERATION AND AQUATIC ECOSYSTEMS RESTORATION

Tese apresentada ao Programa de Pós-graduação em Recursos Hídricos e Saneamento Ambiental da Universidade Federal do Rio Grande do Sul, como requisito à obtenção do grau de doutor(a).

Aprovado em: Porto Alegre, 03 de agosto de 2023.

Prof. Dr. Guilherme Fernandes Marques – UFRGS
Orientador

Prof. Dr. Amaury Tilmant – Université Laval
Coorientador

Prof. Dr. Patrick Reed – Cornell University
Examinador

Prof. Dr. Walter Collischonn – UFRGS
Examinador

Prof. Dr. Francisco Souza de Assis Filho – UFC
Examinador

FINANCING SOURCES AND INSTITUTIONS

This doctoral dissertation was financed by the Inter-American Institute for Global Change Research (IAI) under the SGP-HW program, project SGP-HW 091 and Conselho Nacional de Desenvolvimento Científico e Tecnológico (CNPq) through grant 404242/2019-7.

AKNOLEDGEMENTS

I would like to express my gratitude to all the collaborators and co-authors of the papers resulting from this doctoral dissertation, as well as the institutions they are affiliated with. Their valuable time and knowledge were shared to contribute to ideas, methodology, and discussions on findings.

Guilherme Fernandes Marques (UFRGS), Amaury Tilmant (Universite Laval), Anielly Galego de Oliveira (UEM), Angelo Antonio Agostinho (UEM), Emilio Carlos Prandi (Comitê Paranapanema), Vahid Spanmanesh (Universite Laval), Marcelo Olivares (Universidad de Chile), Yvonilde Dantas Pinto Medeiros (UFBA), Water Collischonn (UFRGS), João Paulo Lyra Fialho Brêda (UFRGS), Rodrigo Cauduro Dias de Paiva (UFRGS), Paulo Yoshio Kubota (INPE), Alexandre Abdalla Araujo (ANA), Olavo Correa Pedrollo (UFRGS), Juliano Santos Finck (UFRGS), Iporã Brito Possantti (UFRGS), Luísa Lucchese (UFRGS), Josue Medellín-Azuara (UC Merced), Joshua Viers (UC Merced).

I am also thankful to NUPELIA (Universidade Estadual de Maringá), which provided support for the study through infrastructure and local access, as well as essential data about fish monitoring. Additionally, I extend my gratitude to the committee members, Walter, Patrick, and Francisco, for whom I feel deeply honored to have evaluated this study and for their valuable contributions.

"There are some problems where inferential evidence is all that we will have; where once the catastrophe arrives it is too late to deal with it." - Carl Sagan in "Broca's Brain: Reflections on the romance of science."

ABSTRACT

The growing demands for water, food and energy, in addition to the need to protect ecosystems, pose significant challenges to water management and the operation of water systems. In hydropower-dominated basins, where reservoirs capture flow variability for energy generation, the modification of the natural flow regime disrupts the natural equilibrium of aquatic ecosystems. Migratory fish species and the associated ecosystem services are particularly vulnerable as the migration and recruitment success relies on the synchronization between the hydrologic flow regime and the reproductive cycle. While there is a consensus on the importance of restoring impacted ecosystems in balance with multiple uses, the current water governance framework lacks a comprehensive understanding of the tradeoffs involved and mechanisms for ensuring the equitable distribution of the adaptation costs among users. The present study brings a contribution to the field by proposing solutions to improve the water governance of river basins, combining the (1) identification of flow-ecological relationships by measuring the response of multiple options of flow regime restoration with a clear ecosystem indicator, (2) incorporation of the flow-ecological relationships and hydroclimatic conditions into the operation decisions of hydropower systems to create dynamic environmental flow solutions (termed Dynamic Adaptive Environmental flows – DAE-flows) with better long-term performance, (3) calculation of the reoperation trade-offs between alternative levels of environmental flow regime restoration and (4) development of mechanisms to share the adaptation costs among stakeholders. The electricity market is proposed as an institutional arrangement and financing mechanism to support the restoration of flow regimes in environmentally sensitive areas. The Upper Paraná River Basin, in Brazil, where consecutive hydropower impoundments have reduced the original floodplain along the last decades, is a recurrent example where reservoirs' operation need to be reconciled with ecosystem functionality, which makes the basin an important study area. The findings of this dissertation indicate that it is possible to enhance the capacity of water systems to incorporate historically suppressed environmental water demands without imposing a hard constraint to economic uses. The consideration of the long-term effects of operation when designing operating strategies for multiple users leads to improved performance in both hydropower generation and meeting ecosystem demands. So, during severe droughts the water can still be reallocated to hydropower (as it is currently done) but at a lesser cost to the environment.

Keywords: environmental flows, water resources management, ecosystem restoration, hydropower planning, multiobjective optimization, climate change

RESUMO

As demandas crescentes por água, alimentos e energia, além da necessidade de proteger os ecossistemas, tornam a gestão dos recursos hídricos, bem como a operação de sistemas hídricos, uma tarefa desafiadora. Em bacias com aproveitamento hidrelétrico, a modificação do regime de vazões decorrente da operação dos reservatórios altera o equilíbrio natural dos ecossistemas aquáticos. Espécies migratórias de peixes e serviços ecossistêmicos associados ficam particularmente vulneráveis, uma vez que o sucesso da migração e recrutamento depende da sincronização entre o regime de vazão e o ciclo reprodutivo. Embora haja consenso sobre a importância de restaurar as demandas ecossistêmicas suprimidas e alcançar um equilíbrio que permita múltiplos usos, o atual quadro de governança carece de uma compreensão abrangente dos *trade-offs* envolvidos e dos mecanismos para garantir a distribuição equitativa dos custos de adaptação entre os usuários. O presente estudo contribui para o campo, propondo soluções para aprimorar a governança de bacias antropizadas, combinando (1) a identificação das relações vazão-ecológicas por meio da quantificação da resposta de múltiplas opções de restauração do regime de vazão por meio de um indicador de desempenho do ecossistema, (2) a incorporação dessas relações vazão-ecológicas juntamente com condições hidroclimáticas nas decisões operacionais de sistemas hidrelétricos (denominadas Vazões Ambientais Dinâmicas e Adaptativas - DAE-flows) para criar soluções dinâmicas de operação de reservatórios, (3) o cálculo dos *trade-offs* de reoperação de múltiplos níveis de restauração de regime de vazão ambiental e (4) o desenvolvimento de mecanismos para compartilhar os custos relacionados entre as partes interessadas. Nesse sentido, o mercado de eletricidade é proposto como arranjo institucional e mecanismo de financiamento para apoiar a restauração de regimes de vazão em áreas ambientalmente sensíveis. A Bacia Hidrográfica do Alto Paraná, Brasil, caracterizada como uma das mais represadas da América do Sul, com 65 usinas hidrelétricas integradas ao Sistema Integrado Nacional, é um exemplo recorrente da necessidade de reconciliação entre a geração de energia e a conservação de serviços ecossistêmicos, sendo utilizada como área de estudo. Os resultados indicam que podemos aumentar a capacidade dos sistemas hídricos para incorporar demandas ambientais historicamente suprimidas sem impor uma restrição rígida aos usos econômicos. Ao considerar os efeitos de longo prazo da operação ao projetar estratégias de operação para múltiplos usuários, obtemos um desempenho aprimorado tanto na geração de energia hidrelétrica quanto no atendimento às demandas do ecossistema. Assim, durante períodos de seca severa, a água ainda pode ser realocada para a produção de energia hidrelétrica (como é feito atualmente), porém com menor impacto ambiental.

Palavras-chaves: vazões ambientais, gestão de recursos hídricos, recuperação de ecossistemas, planejamento de sistemas hidrelétricos, otimização multiobjetivo, governança de bacias antropizadas

SUMMARY

CHAPTER 1

Introduction

1.1 Introduction

Water rights and infrastructure have traditionally been allocated and expanded to meet specific water demands at the lowest cost, often disregarding the benefits of environmental services. Today, water systems worldwide face the challenge of addressing aging infrastructure, meeting growing demands competing for water, and restoring suppressed ecosystems, amidst the uncertainties imposed by a changing climate (OECD, 2015b; UNESCO, 2012).

Reservoir systems, while essential for balancing water (and energy) demand and supply, have altered natural flow regime patterns through the manipulation of storage and release (Maskey et al., 2022). For many migratory fish species, whose recruitment success depends on the synchronization between flow regime and reproductive cycle, the modification of downstream flow results in a functional simplification of the ichthyofauna, leading to a considerable reduction of habitats and aquatic species (Oliveira et al., 2018; Santana et al., 2016). The provision of ecosystem services linked to fish production, such as professional fishing and ecological tourism, has been also affected, bringing social and economic impacts to local communities (Holmlund e Hammer, 1999).

Although operational rules have been established to guarantee a minimum flow downstream of reservoirs, they often fail to consider the dynamics of the natural flow regime required for ecosystem functionality (Basto et al., 2020). Understanding the critical components of the environmental flow regime (e.g., magnitude, frequency, duration, timing and rate of change) necessary to maintain sensitive ecological functions, as the example of fish migration and reproduction, provides a valuable framework for ecosystem restoration plans, surpassing the limitations of minimum flow magnitude approaches (Collischonn et al., 2006; Poff et al., 1997; Yarnell et al., 2015).

However, effective implementation of environmental flows in anthropized and regulated water systems depends on reservoir operation. Changing the latter requires addressing a broader water governance to improve understanding of ecosystem performance, tradeoffs to multiple users, and propose mechanisms for implementation (Hannah et al., 2007; Petts et al., 2006). As restoring natural flow components is a water allocation problem, it presents technical, economic and social-political dimensions (Tonkin et al., 2019). In hydropower-dominated basins, the restoration of flow regime components may result in energy generation disturbances and economic losses (Brambilla et al., 2017; Marques & Tilmant, 2018).

In this context, while the impacts to the ecosystem due to reduced variability of natural flows have been better understood, far less known is how to address the issue with effective water management policies. It remains unclear (a) how environmental flow regimes could be designed as operating policies, (b) how to translate different operations into measurable environmental performance, (c) which are the tradeoffs to multiple users associated to different operations and hydroclimatic conditions, and (d) how to mitigate and fairly distribute those tradeoffs among the different users in the systems.

The present study contributes to the field by addressing the knowledge gaps (a) through (d) above by proposing a methodology framework capable of:

- Creating multiple reservoir operation solutions with known functionality in restoring specific components of a natural flow regime and predicting their environmental performance;

- Evaluating the trade-offs of each solution against multiple system objectives;
- Sharing the trade-off costs among different users; and
- Supporting the definition of agreements and water and energy management instruments and policies.

The Upper Paraná River Basin, in Brazil, where consecutive hydropower impoundments have reduced and modified the original floodplain dynamics along the last decades, is a recurrent example where reservoirs' operation need to be reconciled with ecosystem functionality (Agostinho et al., 2007; Oliveira et al., 2018). The section between the Porto Primavera and the Itaipu dam is the last remaining dam-free lotic environment in the Upper Paraná River Basin, still preserving natural characteristics for spawning and fish growth. However, the inundation dynamics of the floodplain and the success of fish recruitment rely on the decision-making regarding the operation of upstream hydropower reservoirs, which is primarily driven by hydropower objectives.

Despite research findings emphasizing the importance of this issue, the evaluation of reservoir reoperation and financing mechanisms to restore impacted environmental processes is yet to be conducted (Agostinho et al., 2007). This makes the basin an important area to implement the proposed approach. The availability of data, including river flows, ecosystem data (e.g., fish population), reservoir operating rules, and water demands, was another crucial aspect considered when selecting this study area.

1.2 Goal and Objectives

The main objective of this dissertation is to improve the governance of river basins, exploring adaptation pathways to reconcile hydropower production with the restoration of ecosystem functions already at risk. To achieve this goal, four specific objectives are proposed.

1. The first is to improve the quantitative understanding of the ecosystem response to different combinations of flow regime components.
2. The second is to design environmental flow policies capable of improved long-term economic and ecosystem performance under multiple hydroclimatic conditions.
3. The third is to calculate the hydropower trade-offs to meet different levels of environmental flow regime restoration.
4. The fourth is to develop mechanisms to share the adaptation costs among stakeholders, capable of delivering the solutions to the field.

1.3 Study area

The Upper Paraná River Basin is one of the most impounded of South America with 65 hydropower plants and a generation installed capacity of 48,381 MW, which corresponds to about 40% of the total Brazilian hydropower generation (ANA, 2020; CCEE, 2020). Within this basin, the reach of the Paraná River spanning 230 km between the Porto Primavera dam and the Itaipu reservoir represents the last remaining dam-free lotic environment of the original floodplain (Figure 1) (Oliveira et al., 2015).

This particular river segment is affected by the operation of 56 hydropower plants upstream and 8 hydropower plants downstream from the Itaipu hydropower plant (ANA, 2020). While the floodplain still maintains some natural characteristics essential for fish spawning and

migration, the restoration and maintenance of related ecosystem services require reoperation of the reservoirs, and the associated tradeoffs are not yet well understood.

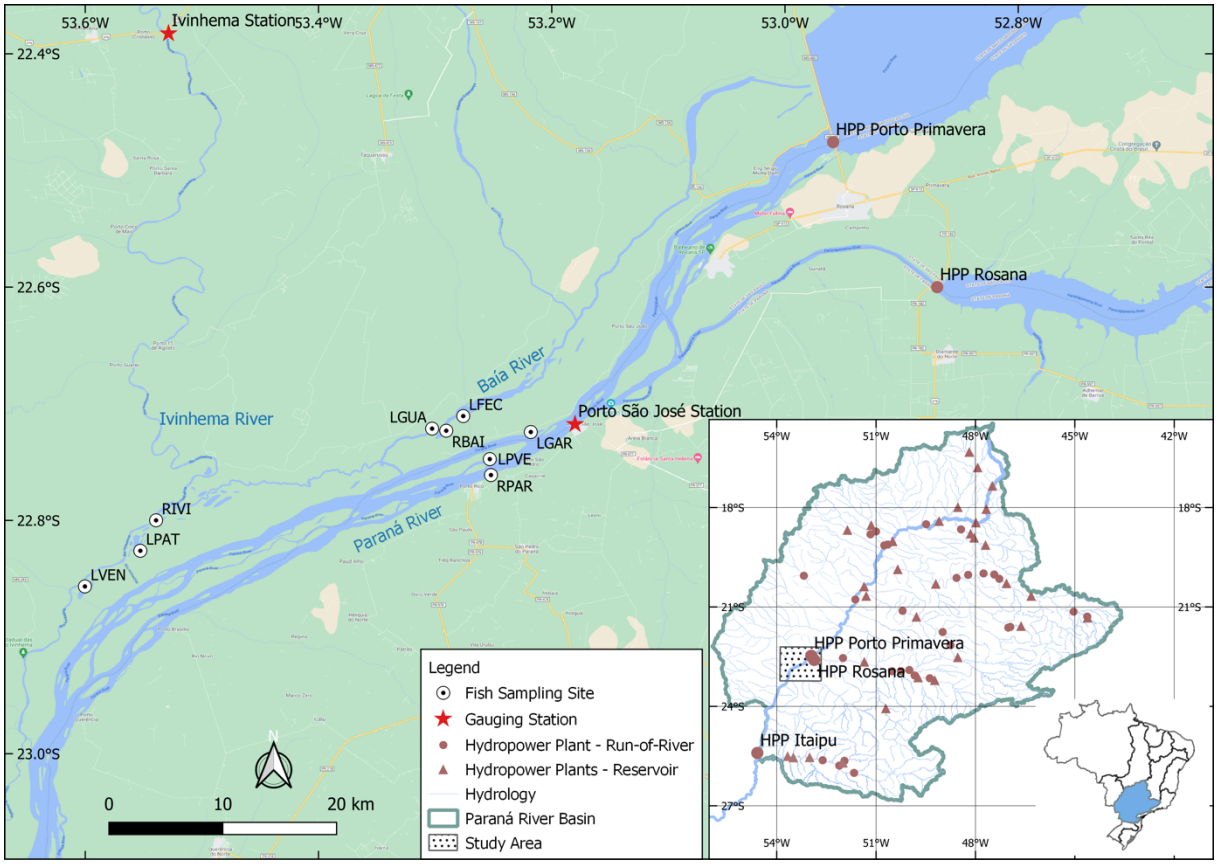

Figure 1. Upper Paraná River Floodplain, including the fish sampling and flow gauging stations.

Studies in this area have identified a simplification of the fish functional diversity as a consequence of alterations in the natural flow caused by hydropower operations (Oliveira et al., 2018; Suzuki et al., 2009). Figure 2 compares the functional richness (FRic), Rao's quadratic entropy (FDQ) and functional redundancy (FRed) before (1986-95) and after dam construction and operation (2000-2015), indicating a decrease in mean values of functional richness and entropy and an increase in the functional redundancy.

The study in Oliveira et al. (2018) also points out that functional traits associated with the pre-intervention period are related to large species that perform long-distance reproductive migrations, inhabit pelagic habitats, and possess superior or subterminal mouths. These traits are commonly found in rheophilic species that have a strong dependency and synchrony between the hydrological cycle and the reproductive cycle. As a result, they are more susceptible to the negative impacts of flow regulation caused by dams. Furthermore, these species often hold a high commercial value and are significant for human consumption.

In contrast, the traits that contributed the most to the post-intervention period are typical of non-migratory species that usually inhabit lentic environments. These traits include parental care, an omnivorous diet, and a benthopelagic habitat.

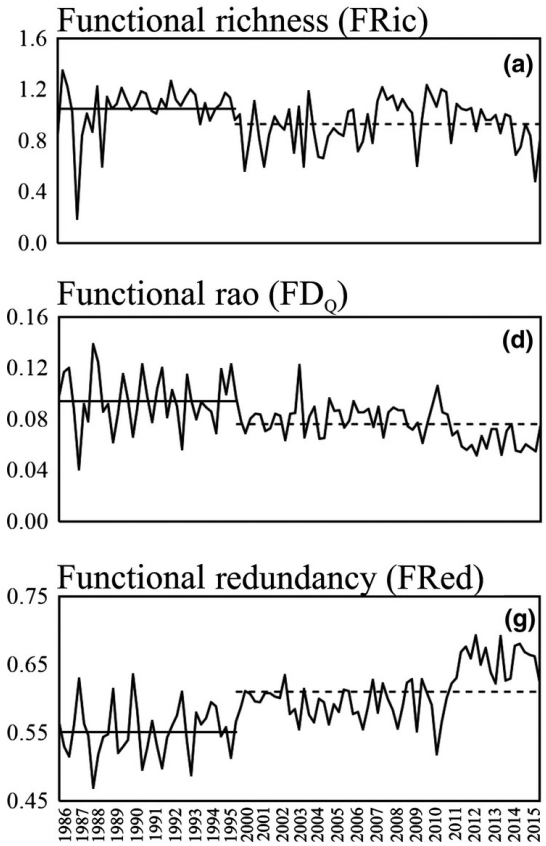

Figure 2. Functional biodiversity indexes in the Upper Paraná River floodplain. Adapted from: (Oliveira et al., 2018).

The ecosystem impacts also reflect on people's livelihood in the region. During a field trip conducted as part of the research work, a fishing organization interviewed in the study area reported a significant decline in membership. The association had 1200 members in 2010, but this number dropped to 384 members in 2019, representing a 68% decrease over the past 10 years. Many fishermen have reported a reduction in the abundance of high-value migratory species, expressing difficulties in sustaining their livelihoods through fishing practices. As a result, many have been compelled to either abandon fishing altogether and shift to alternative activities.

Recent severe droughts have also posed operational challenges for hydropower plants in the area. During the 2021-2022 drought, the Porto Primavera hydropower plant (part of the Paraná cascade) had to adopt emergency measures to maintain sufficient storage levels for hydropower production in the basin. As a result, the Porto Primavera minimum releases for the downstream floodplain were reduced from 4600 m^3/s to 2900 m^3/s (ONS, 2022).

Such management approaches tend to prioritize meeting high-priority (economic) demands at the expense of the environment, which is often the first to be sacrificed. The dam operational adjustment during the last drought indicates that there is still a need to further explore alternative solutions to reconcile economic demands and the environment, their tradeoffs and the strategies to implement the solutions. This will contribute to better preparedness of the water system to face the incoming droughts, reducing the impacts for both the ecosystem and the hydropower system.

1.4 Chapters organization

This doctoral dissertation is divided in seven main chapters, with each contributing to address the knowledge gaps and objectives outlined. Figure 3 presents the general flowchart of the dissertation.

Chapter 2 introduces the framework proposal for establishing flow-ecological relationships. It involves constructing an ensemble of flow regime options by considering the variability of the naturalized flow regime range. The framework then quantifies the ecosystem response of each flow regime option in terms of migratory fish abundance using an artificial neural network model.

Chapter 3 outlines the modeling framework employed to simulate the hydropower system operation in the study area. This framework utilizes the explicit stochastic dual dynamic programming method. A performance analysis is conducted to evaluate the simulation results in comparison to observed data.

Chapter 4 introduces hydroclimatic scenarios for the purpose of measuring the operational adaptive capacity of the system to mitigate climate change impacts. It further evaluates independent and combined impacts of climate change and system operation on the aquatic ecosystem, while also examining optimized operating policies in response to a changing climate.

Chapter 5 explores the design of environmental flows (e-flows) as dynamic operating policies. It investigates how multiple flow regime options can be combined throughout a planning horizon to strike a balance between immediate and future water use benefits and produce different levels of ecosystem performance. The resulting trade-offs between different levels of ecosystem performance and hydropower production is examined.

Chapter 6 outlines a cost-sharing mechanism, which considers the electricity market as an institutional and financing arrangement for restoring flow regimes in environmentally sensitive areas.

Chapter 7 explores a supporting work developed during the doctorate period as part of a CNPq project and to study the influence of hydro-meteorological forecasts on the production and economic revenue of hydropower systems. While this chapter does not directly relate to the primary objectives of the dissertation or its methodological structure, it incorporates several methodological approaches derived from this dissertation that identified valuable insights for future studies on how hydropower systems can benefit from improved hydrometeorological data and forecasts. In future studies, such improvement can support further refinement on the proposed environmental flow solutions.

Chapter 8 presents a conclusive summary of the findings and learnings of this dissertation.

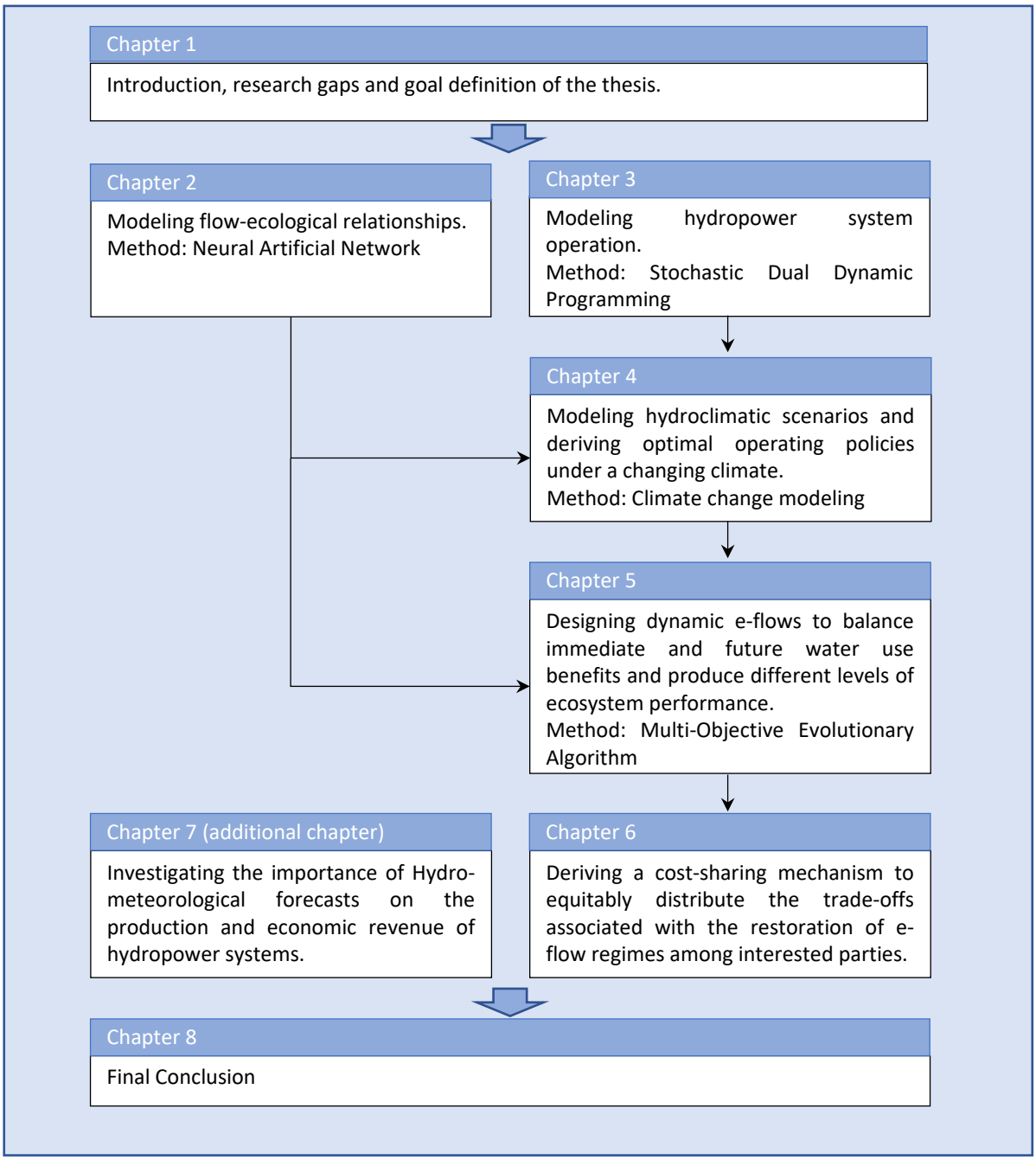

Figure 3. General flowchart of the proposed methodology framework.

1.5 References

Agência Nacional de Águas (ANA). (2020). SAR - Sistema de acompanhamento de reservatórios. Retrieved from https://www.ana.gov.br/sar/

Agostinho, A. A., Pelicice, F. M., Petry, A. C., Gomes, L. C., & Júlio, H. F. (2007). Fish diversity in the upper Paraná River basin: habitats, fisheries, management and conservation. Aquatic Ecosystem Health & Management, 10(2), 174–186. https://doi.org/10.1080/14634980701341719

Basto, I. D. R. G., Fontes, A. S., & Medeiros, Y. D. P. (2020). Effects of an outflow regime adoption of the São Francisco River reservoir system to meet water demands for multiple uses. RBRH, 25. https://doi.org/10.1590/2318-0331.252020190110

Brambilla, M., Fontes, A. S., & Medeiros, Y. D. P. (2017). Cost-benefit analysis of reservoir operation scenarios considering environmental flows for the lower stretch of the São Francisco River (Brazil). RBRH, 22. https://doi.org/10.1590/2318-0331.0117160014

CCEE. (2020). Hydroedit - apoio à leitura de arquivos. Retrieved December 10, 2020, from https://www.ccee.org.br/acervo-ccee?especie=44884&keyword=hydroedit&periodo=5000

Collischonn, W., Agra, S., Freitas, G., & Priante, G. (2006). Da Vazão Ecológica ao Hidrograma Ecológico. 8o Congresso Da Água.

Hannah, D. M., Sadler, J. P., & Wood, P. J. (2007). Hydroecology and ecohydrology: a potential route forward? Hydrological Processes, 21(24), 3385–3390. https://doi.org/10.1002/hyp.6888

Holmlund, C. M., & Hammer, M. (1999). Ecosystem services generated by fish populations. Ecological Economics, 29(2), 253–268. https://doi.org/10.1016/S0921-8009(99)00015-4

Marques, G. F., & Tilmant, A. (2018). Cost Distribution of Environmental Flow Demands in a Large-Scale Multireservoir System. Journal of Water Resources Planning and Management, 144(6), 04018024. https://doi.org/10.1061/(ASCE)WR.1943-5452.0000936

Maskey, M. L., Facincani Dourado, G., Rallings, A. M., Rheinheimer, D. E., Medellín-Azuara, J., & Viers, J. H. (2022). Assessing Hydrological Alteration Caused by Climate Change and Reservoir Operations in the San Joaquin River Basin, California. Frontiers in Environmental Science, 10. https://doi.org/10.3389/fenvs.2022.765426

OECD. (2015). Water Resources Governance in Brazil. Paris: OECD. https://doi.org/10.1787/9789264238121-en

Oliveira, A. G., Suzuki, H. I., Gomes, L. C., & Agostinho, A. A. (2015). Interspecific variation in migratory fish recruitment in the Upper Paraná River: effects of the duration and timing of floods. Environmental Biology of Fishes, 98(5), 1327–1337. https://doi.org/10.1007/s10641-014-0361-5

Oliveira, A. G., Baumgartner, M. T., Gomes, L. C., Dias, R. M., & Agostinho, A. A. (2018). Long-term effects of flow regulation by dams simplify fish functional diversity. Freshwater Biology, 63(3), 293–305. https://doi.org/10.1111/fwb.13064

ONS. (2022). Manual de Procedimentos da Operação - Módulo 5 - Submódulo 5.11 - CD-OR.PR.PAR. Brasil. Retrieved from https://www.ons.org.br/%2FMPO%2FDocumento Normativo%2F2. Cadastros de Informações Operacionais - SM 5.11%2F2.3. Cadastros de Informações Operacionais Hidráulicas%2FCD-OR.PR.PAR_Rev.73.pdf

Petts, G., Morales, Y., & Sadler, J. (2006). Linking hydrology and biology to assess the water needs of river ecosystems. Hydrological Processes, 20(10), 2247–2251. https://doi.org/10.1002/hyp.6223

Poff, N. L., Allan, J. D., Bain, M. B., Karr, J. R., Prestegaard, K. L., Richter, B. D., et al. (1997). The Natural Flow Regime. BioScience, 47(11), 769–784. https://doi.org/10.2307/1313099

Santana, K. N. C., Torres, C. J. F., Fontes, A. S., Costa, A. R., Peso-Aguiar, M. C., Alcântara Santos, A. C., & Pinto Medeiros, Y. D. (2016). Efeitos da regularização dos reservatórios na ictiofauna do baixo curso do rio São Francisco. Revista Eletrônica de Gestão e Tecnologias Ambientais, 4(1), 95. https://doi.org/10.9771/gesta.v4i1.15080

Suzuki, H., Agostinho, A., Bailly, D., Gimenes, M., Júlio-Junior, H., & Gomes, L. (2009). Inter-annual variations in the abundance of young-of-the-year of migratory fishes in the Upper Paraná River floodplain: relations with hydrographic attributes. Brazilian Journal of Biology, 69(2 suppl), 649–660. https://doi.org/10.1590/s1519-69842009000300019

Tonkin, J. D., Poff, N. L., Bond, N. R., Horne, A., Merritt, D. M., Reynolds, L. V., et al. (2019). Prepare river ecosystems for an uncertain future. Nature, 570(7761), 301–303. https://doi.org/10.1038/d41586-019-01877-1

UNESCO. (2012). O manejo dos recursos hídricos em condições de incerteza e risco. Brasília, DF, Brasil. Retrieved from http://www.ecoa.org.br/wp-content/uploads/2015/10/WWDR4-Fatos-e-Dados.pdf

Yarnell, S. M., Petts, G. E., Schmidt, J. C., Whipple, A. A., Beller, E. E., Dahm, C. N., et al. (2015). Functional Flows in Modified Riverscapes: Hydrographs, Habitats and Opportunities. BioScience, 65(10), 963–972. https://doi.org/10.1093/biosci/biv102

CHAPTER 2

Identifying Functional Flow Regimes and Fish Response for Multiple Reservoir Operating Solutions

This chapter has been published and it can be found under https://doi.org/10.1061/(ASCE)WR.1943-5452.0001567.

2.1 Introduction

Flow regulation through dams represent the most prevalent form of hydrological alteration of rivers with projections to expand in the following decades (Grill et al., 2015; Tharme, 2003). While such alteration is desirable to increase water, food and energy security for society (Tilmant et al., 2014), the consequent disruption of flow regime patterns and reduction of aquatic and wetland habitats contribute to dramatic population declines of aquatic species (Howard et al., 2018; Palmer & Ruhi, 2019). Moyle et al. (2011) estimate more than 80% of California's native fishes are likely to be lost in the next 100 years if changes in water management are not made and negative effects of climate change are not averted or reversed.

Because maintaining or restoring full natural flow regimes to mitigate impacts is usually unfeasible or undesirable, the concept of environmental flows has emerged to strike a balance between economic uses of water and ecosystem preservation (Poff et al., 2017). This idea explores the wide range of flow regime options that can be preserved or restored to some society preferred condition, both in already altered rivers or where new water infrastructures are planned (Arthington et al., 2018).

Choosing between flow regime options, however, requires capacity to predict ecological, technical, social, and economic outcomes (Arthington et al., 2018). Hydropower reservoir reoperation incorporating environmental water needs often reduces generation capacity, leading to reliability and economic losses to the power sector, while water supplies may also be reduced, forcing municipalities and irrigation districts to seek out more expensive sources (Adams et al., 2017; Crespo et al., 2019). Managing such implications is still a challenge to implement environmental flows in a holistic perspective (Poff et al., 2017), resulting in few examples that go beyond a minimum flow requirement (Harwood et al., 2017; Quesne et al., 2010).

Therefore, obtaining a better quantitative understanding of ecological responses to different levels of flow regime restoration is critical for evaluating the range of economic losses and engaging stakeholders in decision-making. This process starts with characterizing the natural flow variability through its critical components, such as magnitude, timing, duration, frequency, and rate of change (Poff et al., 1997; Olden & Poff, 2003), followed by understanding the ecological response to the natural variability and degrees of alteration (Arthington et al., 2006), to finally calculate the trade-offs to other uses (Chen & Olden, 2017; Li et al., 2020; Suen & Eheart, 2006; Wild et al., 2019) and propose adaptation costs distribution among users (Marques & Tilmant, 2018a).

Focusing on flow regime components that trigger significant geomorphological and ecological processes (also termed functional flow regimes) provides a strategic frame of reference to develop ecological-flow relationships and more successful restoration plans (Grantham et al., 2020; Yarnell et al., 2015). Fish are part of food web dynamics and nutrient cycling, serving as an effective indicator of ecosystem health with the advantage of being sensitive to flow dynamic changes (Whitfield & Elliott, 2005). Many studies evaluating the modification of downstream flow regimes by reservoirs' regulation highlight a simplification of the ichthyofauna diversity, with a marked reduction in migratory species (Cooper et al., 2017; Loures & Pompeu, 2018; Pringle et al., 2000). Fisheries also represent a traditional ecosystem service provision (e.g., food and ecotourism), contributing to social and economic activities (Holmlund & Hammer, 1999).

Statistical approaches have been applied as means to quantify and interpret meaningful flow regime components that drive ecological processes to sustain fish populations and communities. Studies as Freeman et al. (2001), Oliveira et al. (2015), Piffady et al. (2010), Tonkin et al. (2021) and Wang et al. (2019) statistically analyzed the degree of fish response to flow regime indices, showing that the intensity, timing and duration of flood pulses when synchronized with the life stages during the spawning and recruitment processes are highly correlated with juveniles' abundances. Floods trigger fish migration for spawning and connect longitudinally and laterally different habitats across the floodplain, providing feeding and refuge conditions for initial growth. By retaining high flows during the rainy season to make it available during the dry season, reservoir regulation reduces or eliminates flood peaks, while higher flow periods are artificially created in the dry season. Fish recruitment is then affected.

With the advancements of machine learning techniques, data-driven models have also been applied to empirically model complex systems by extracting fish patterns from historical datasets. A set of environmental variables, including flow regime components, is used to predict, as examples, spatial fish occurrence (Joy & Death, 2004), fish biodiversity (Hu et al., 2020) and fish recruitment probability (Fernandes et al., 2010).

Despite recent innovation, water managers still face a knowledge gap to translate the set of components of a flow regime to restore key ecological functions into objectives (McKay et al., 2012) and reservoir operating practices, as the latter need to accommodate other multi-objective demands (e.g., hydropower, irrigation, and urban supply). Fish are adapted to a certain level of flow variability and, given the wide range of flow regime options when dealing with flow regime restoration, choosing which ones to address with reservoir operation can yield different impacts on the water system reliability and expenses. Although such impacts can be measured between tangible economic uses, the ecosystem response performance is still largely unknown.

This chapter addresses this knowledge gap with a methodology framework that explicitly quantifies the response of different flow regime options towards a key ecosystem function to guide the formulation of environmental flows. In the case of the study area, this function is the recruitment success of migratory fish species. The framework combines three main parts. In the first subroutine, an ensemble of flow regime options is produced based on the naturalized flow regime range variability. The second subroutine derives a set of flow metrics (indices) to quantify the five main components (magnitude, timing, duration, frequency, and rate of change) of each flow regime option. The third subroutine contains an Artificial Neural Network (ANN) predictive model that calculates the response of migratory young-of-the-year (YoY) fish abundance of each flow regime option using the corresponding flow regime indices as predictors. The options with positive non-zero responses were termed functional flow regimes (or functional flows) as they provide conditions to support the recruitment success of migratory fish species.

2.1.1 Study area: Flooding dynamics and ichthyofauna behavior

The daily level of the Paraná River is registered by the Porto São José gauging station (id 64575003) (ANA, 2020). Flood events exclusively influenced by the Paraná River can fully submerge the floodplain, creating connections between various habitats, such as lagoons and secondary channels (Comunello et al., 2003). Other two tributaries influence the floodplain inundation dynamic, the Baía and Ivinhema tributaries, although reaching narrower floodplain

coverage. Combined events, when Paraná River flooding is concomitant with tributaries flooding, are also observed.

The ichthyofauna of Upper Paraná River is composed of 211 cataloged species, which can be categorized into two major groups: sedentary/short-distance migratory and long-distance migratory (Ota et al., 2018). Long-distance migratory species are characterized by having larger size and longer lifespan, requiring different habitats during their life cycle for spawning, early development and feeding (Agostinho et al., 2007). Three main movements characterize the relation between the long-distance migratory fish reproduction cycle and the flow regime in the study area (Agostinho et al., 2007; Oliveira et al., 2015).

At the beginning of the rainy season, a combined increase in the photoperiod and temperature triggers gonadal development and schools' formation. This is followed by an upstream migration (from October to November) when fish schools move to upstream reaches and tributaries, where eggs are laid and can develop in well oxygenated waters with lower predation risk. High water levels (from January to March) promote the connectivity between different habitats (lagoons, channels, etc.), which enables the lateral movement of the larvae along the floodplain area for feeding and refuge. The last movement occurs during decreasing water levels (from March to May) and allows the backward movement towards the main river channel.

The period of low waters occurs during winter (June to September). During this phase, floodplain habitats are less connected with rivers and subject to local processes like wind turbulence, thermal mixing, and inputs from small tributaries, which influence variations of physicochemical parameters and vegetation growth (Agostinho et al., 2000).

2.1.2 Fish sampling data

Fish sampling data spans quarterly from March to December from 2000 to 2019 at nine sampling sites within the floodplain (Figure 1), including three rivers (Paraná River and Ivinhema and Baía tributaries) and two adjacent lagoons for each river, as reported in Oliveira et al. (2015) and Oliveira et al. (2020). The grouping of each river and its corresponding lagoons was termed a sub-system. Data from previous years are reported in Suzuki et al. (2009) with intermittent periods from 1987 to 1988 and 1992 to 1994. To construct the complete dataset, we selected the years 1992 to 1994, combined with the years 2000 to 2019, as both periods provide available data for the same species in all fish campaigns.

Five long-distance migratory fish species were considered: *Brycon orbignyanus* (Valenciennes 1850), *Pseudoplatystoma corruscans* (Spix & Agassiz 1829), *Pterodoras granulosus* (Valenciennes 1821), *Prochilodus lineatus* (Valenciennes 1837), *Salminus brasiliensis* (Cuvier 1816), which are the most abundant among the long-distance migratory fishes, representing almost 25% of the total number of migratory species in the Paraná River Basin. The abundance of young-of-the-year (YoY) fish individuals, which represents the recruitment success of the last flood season (Figure 4), was determined by counting the number of individuals within specific length ranges up to one year of age (Oliveira et al., 2020) and indexed as Catch Per Unit Effort (CPUE; individuals/1000 m^2 of gillnets during 24h).

The annual YoY fish abundance of each sub-system was represented as the average between the corresponding sampling sites. To represent the annual YoY fish abundance of the floodplain related to the Paraná river flow regime (Porto São José Gauging Station), the fish abundance average between sub-systems was considered when combined flood events occurred during the

rainy season. To avoid overestimating fish abundance due to tributaries' flooding, floodplain fish abundances were set to zero when flood events were registered only in the tributaries. Finally, for years when flood events were registered exclusively at the Paraná River, the average between sub-systems considered the tributaries' abundances as zero. Figure 9 presents the total annual YoY fish abundance for the floodplain.

Year	Y-1												Y											
Month	J	F	M	A	M	J	J	A	S	O	N	D	J	F	M	A	M	J	J	A	S	O	N	D
Hydro					Dry season					Rainy season														
Fish															Fish sampling									

Figure 4. Representation of the flooding and fish sampling period.

2.2 Methodology

The methodology framework includes three main subroutines (Figure 5). In the first subroutine, an ensemble of flow regimes options is produced based on the naturalized flow regime range variability of the study area. The flow regime options consist of annual hydrologic time-series of daily level (covering the dry and rainy seasons that occur in an annual period). The second subroutine derives a set of flow metrics (indices) to quantify the five main components (magnitude, timing, duration, frequency, and rate of change) of each flow regime option. The third subroutine contains an Artificial Neural Network (ANN) predictive model that calculates the response of migratory young-of-the-year (YoY) fish abundance of each flow regime option using the set of flow regime indices as predictors. The flow regime options with positive non-zero responses were nominated functional flow regimes.

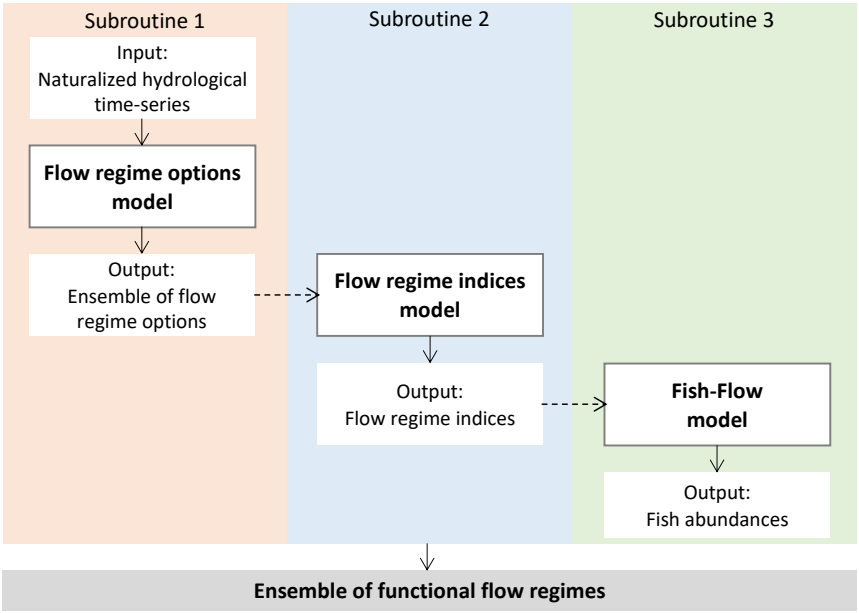

Figure 5. Methodology framework.

2.2.1 Flow Regime Options Model

To generate an ensemble of flow regimes options, the naturalized flow regime was first estimated by reverting the flow regulation effects and evaporation losses from the reservoirs part of the hydropower system. The resulting range of the long-term naturalized flow regime variability appears in Figure 6. The procedure details for its estimation are described in Appendix I.

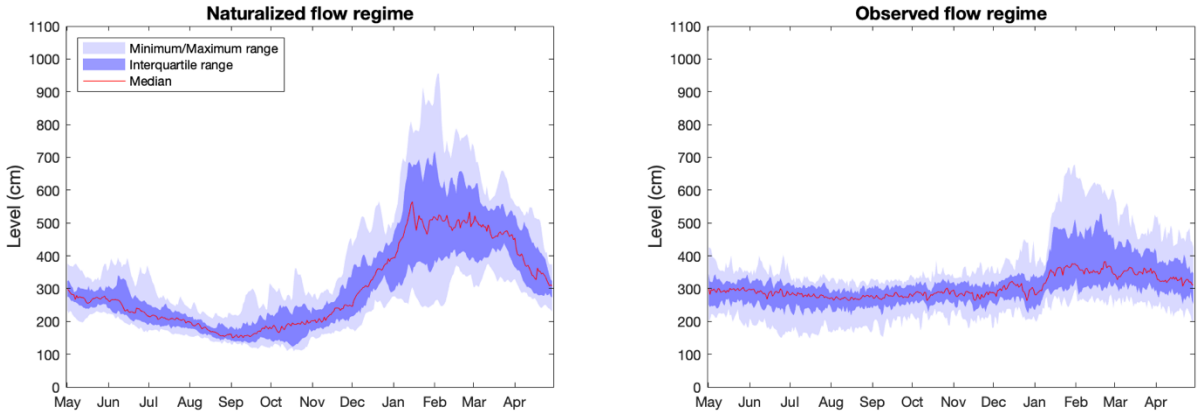

Figure 6. Comparison between the observed and the naturalized flow regime at Porto São José station.

From the naturalized flow time-series, the subroutine adopts a three-step procedure: (1) the daily time-series is converted to a specific time-step (e.g., biweekly or monthly) average time-series and the long-term variability of the given time-step is calculated (Figure 7 - left chart); (2) the range between the minimum and maximum values is divided in discrete states (Figure 7 - middle chart), and (3) combinations between the sequential states are then computed (Figure 7 - right chart). The daily values between the monthly or biweekly time steps are then built by linear interpolation. As a result, an ensemble of annual hydrologic time-series of daily level is generated representing multiple flow regime options. For example, considering a monthly time-step and 5 discrete flow/level states results in the composition of 5^{12} different flow regime options.

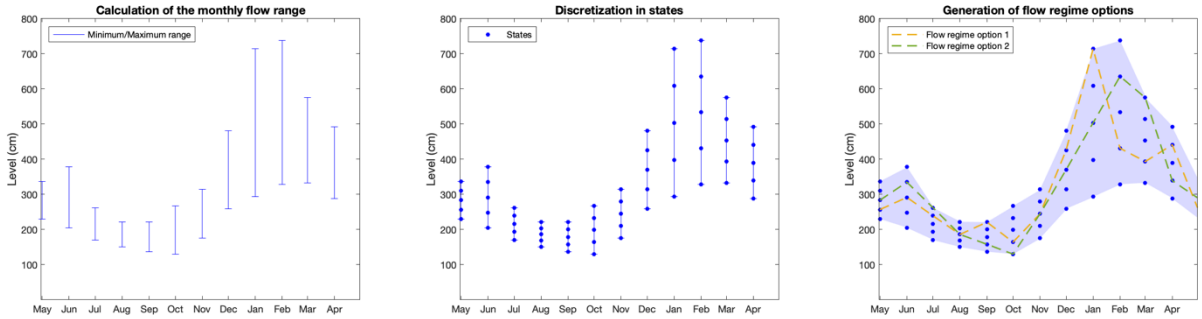

Figure 7. Representation of the generation of flow regime options.

2.2.2 Flow Regime Indices Model

This subroutine calculates flow regime indices (metrics) from the flow regime options generated in subroutine 1. The model represents each component of a flow regime (duration, magnitude, timing, frequency, and rate of change) by indices that must be chosen according to the ecological function modeled. For the study area, nine indices were selected, at least one index for each component (Table 1), to represent the dry and rainy seasons and conditions historically linked to fish migration and initial growth of migratory species.

Table 1. Flow regime indices used to represent the Paraná River reach flow regime.

Flow regime component	Indices	Thresholds
Duration and Magnitude	FSD High magnitude	number of days with "water level >= 610cm" during the rainy season from 01/October to 30/April
	FSD Mid magnitude	number of days with "540cm <= water level < 610cm" during the rainy season from 01/October to 30/April
	FSD Low magnitude	number of days with "450cm <= water level < 540cm" during the rainy season from 01/October to 30/April
	DSD	number of days with "water level <= 250cm" during the dry season from 01/June to 30/September
Magnitude	Maximum magnitude	highest water level (cm) record during the rainy season from 01/October to 30/April
Timing	Flood delay	number of days from 01/October the first flood (water level >=450cm) was recorded
Variability (rate of change)	Flood pulses	number of complete cycles of high (>= 450cm) and low water level during the rainy season from 01/October to 30/April
	Uninterrupted flood duration	longer number of sequential days with "level >= 450cm" during the rainy season 01/October to 30/April
Frequency	Inter-annual flood occurrence	number of previous years without flood (level>=450cm)

The previous studies of Suzuki et al. (2009), Oliveira et al. (2015) and Oliveira et al. (2020) supported the specification of the indices' thresholds. The indices representing the flood season duration (FSD) were divided in three main magnitude ranges in order to represent different floodplain connections during the flood season: (a) the index *FSD Low magnitude* considers the level between 450 and 540 cm as the minimum range to allow lateral and longitudinal connectivity in the floodplain during the rainy season, (b) the index *FSD Mid magnitude* considers the level between 540 cm and 610 cm as the intermediary connectivity, and (c) the index *FSD High magnitude* contemplates the level 610 cm as the threshold level that allows high connectivity along the floodplain.

The dry season duration is represented by the index *DSD*, which considers the level of 250 cm as the water threshold level governed by the baseflow (historical Q_{80} flow duration). The flow regime timing component is represented by the *flood delay* index and the rate of change (variability) is represented by the *uninterrupted flood duration* and the *number of flood pulses* indices. The *uninterrupted flood duration* index indicates how spaced the flood pulses are distributed in time (e.g., long uninterrupted flood duration is produced by time distant pulses). The *inter-annual flood occurrence* index represents the frequency component. The relevance of each index is analyzed in Appendix IV.

2.2.3 Fish-Flow Model

Artificial Neural Networks (ANN) are data-driven computational networks able to establish empirical relationships between independent (input) and dependent (output) variables (Sadiq et al., 2019) with the advantage of not being limited by a pre-specified functional form (Adamowski & Karapataki, 2010). The ANN model developed to predict the YOY fish

abundance from different flow regime options consists of three layers: an input layer, a hidden layer, and an output layer (Figure 8).

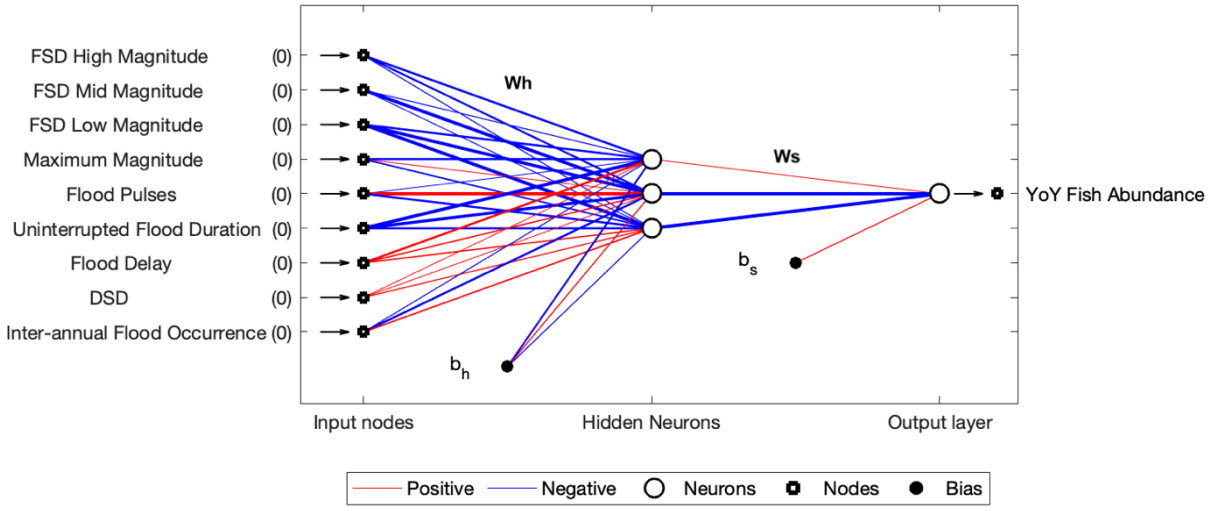

Figure 8. Representation of ANN model architecture.

The input layer has 9 nodes representing the set of annual flow regime indices calculated by the flow regime indices model (subroutine 2). The input layer distributes the input signals via connections to each hidden neuron. Each connection has a weight (w) adjusted via training, and each neuron has an activation function (f). Neurons process the sum of impinging signals from previous layers and independent terms (b), with the activation function, and each output neuron sends its output signal to the respective output node. The output node is represented by the annual YoY fish abundance of the floodplain.

The input and output data are linearly scaled to fit the domain range [0,1] whose scaling parameters are the respective global maximum and minimum of each variable in the dataset. Table 2 summarizes the main parameters used to configure the ANN model. We investigated the number of hidden neurons (hn) necessary to present a performance similar to an oversized ANN by testing different numbers of hidden neurons and evaluating the final overall performance.

Table 2. ANN parameters.

Parameter	Description
Architecture	9 - hn - 1
Input variables	Flow regime indices
Output variable	YoY Fish Abundance
Number of hidden neurons (hn)	3 (choosen according to the complexity analysis)
Activation function	sigmoid unipolar; $f(x) = \frac{1}{1+e^{-x}}$;
Input data scaling	linear (amplitude); [0,1]
Data time step	Annual

To predict the YoY fish abundance from different flow regime options, the ANN model required to be firstly trained and validated based on the historical data. The registers (individual input-output pairs) from 1991 to 1993 and 1999 to 2018 composed the dataset (the year number corresponds to the year the flood season begins - see Appendix II).

To prevent overfitting and to overcome the challenge of working with a small dataset, we applied a Nested Leave-One-Out Cross-Validation (NLCV) training approach (Wong, 2015). This approach (see Appendix III) consisted in using the dataset with different configurations of registers divided between training (TS) and verification (VS) sets and training each configuration separately to check the consistency of the model to produce similar results between configurations, which corroborates its generalization capability to new data. The final dataset was arranged in 3 configurations, each with 6 registers for the verification set and 17 registers for the training set (Figure 9). Years with unique features (Appendix II) were included in the training set to improve model's ability to recognize such behavior.

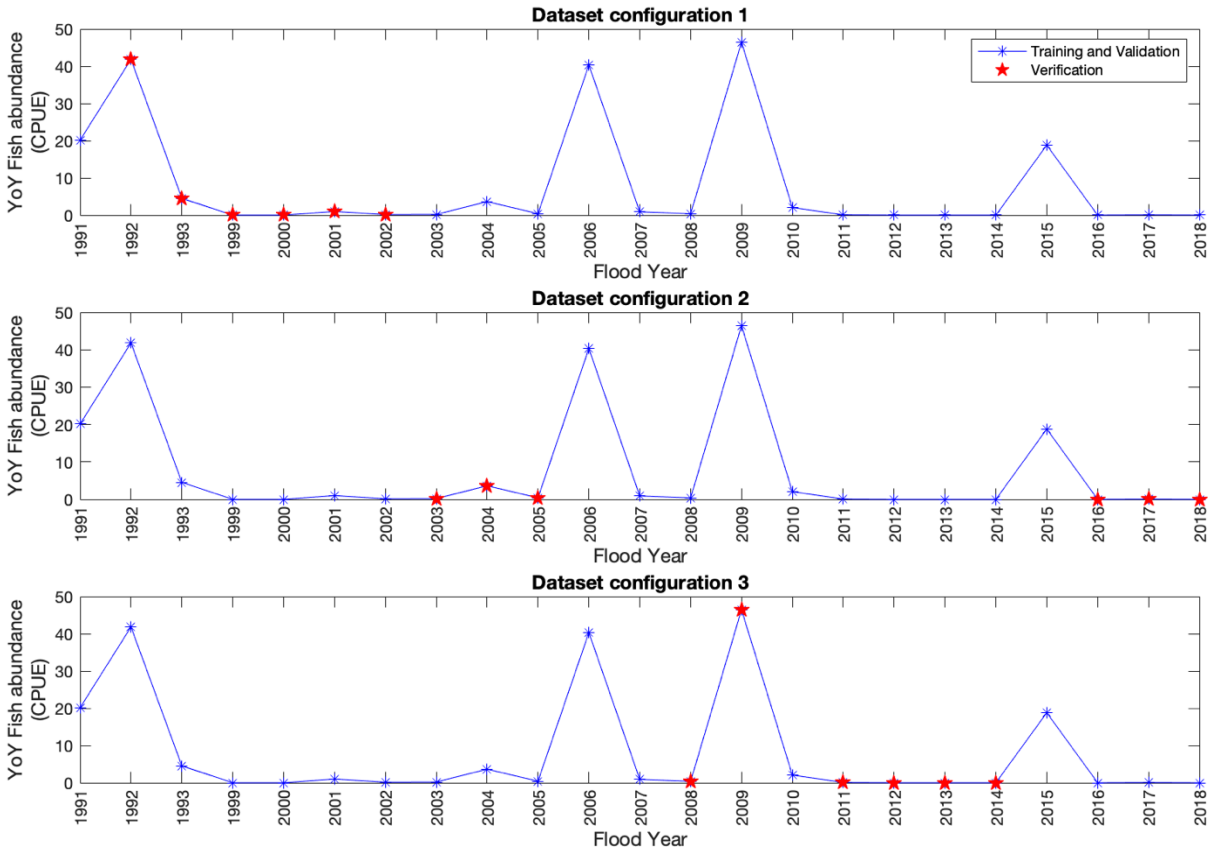

Figure 9. Training and verification registers for each dataset configuration.

The trained ANN model integrated the model subroutine 3 with the objective of calculating the corresponding YOY fish abundance of each flow regime option designed in subroutine 1. To reduce the number of combinations assessed in this study, we discarded flow regime options with very close characteristics in terms of fish abundance and reservoir operation decisions. The final options were termed functional flow regimes, arranged in hydrographs.

2.3 Results and Discussion

2.3.1 Performance Analysis of the Fish Abundance Model

Figure 10 presents the comparison between observed and predicted results for the training and verification sets of the three dataset configurations. Four years of the dataset present unique features, which required them to be included in the training set during the ANN model training and validation to improve model's ability to recognize such behavior. However, it is worth noting that the absence of similar features in the verification set limits our ability to assess the

model's prediction performance in those cases. While the metrics indicate good results, the model's generalizability to new data relies on obtaining more future information and monitoring data.

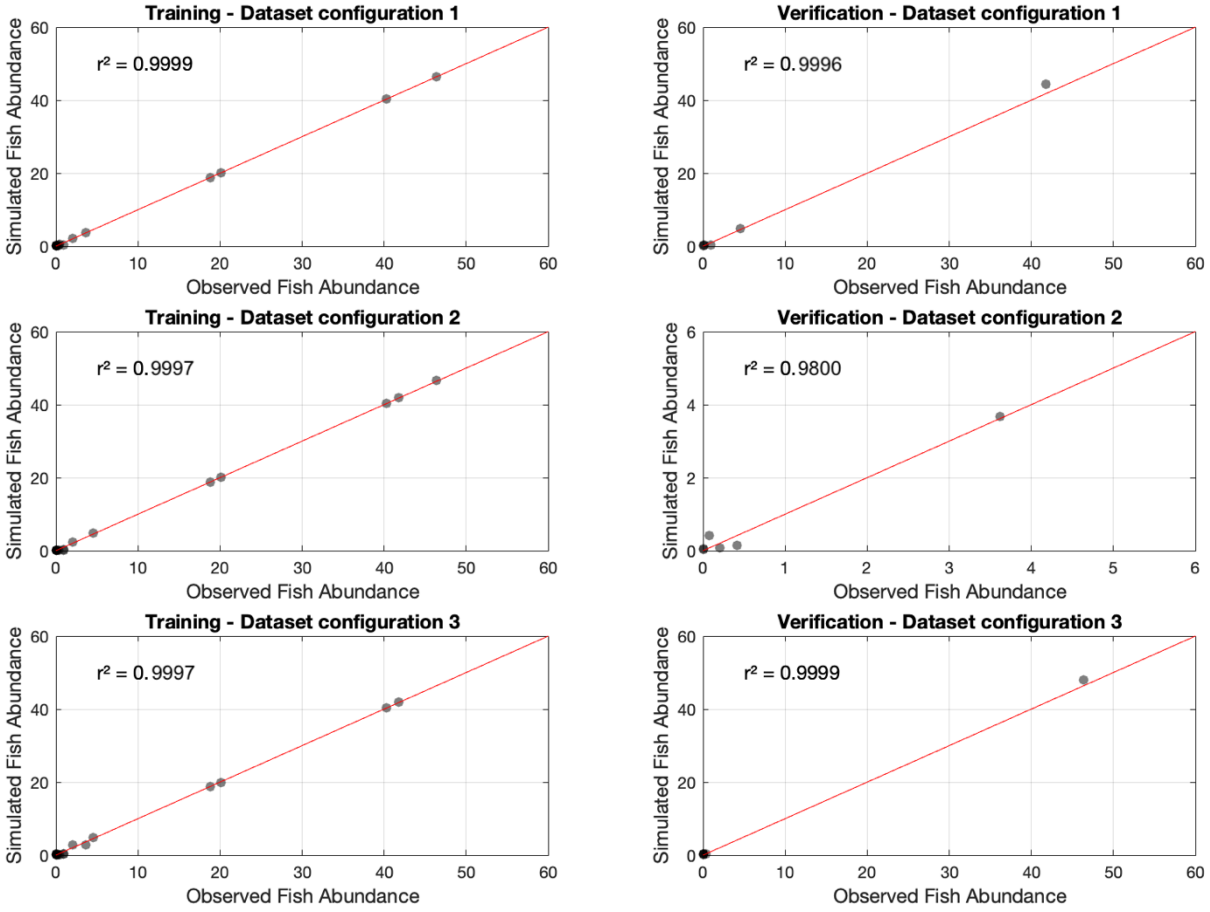

Figure 10. Comparison between predicted and fish abundance for each dataset configuration.

Despite the majority of training data representing YoY fish abundances below 4 CPUE, the ANN model successfully replicated the peak abundance patterns observed in the verification sets. This indicates the model's robustness in defining clear objectives for ecosystem management, specifically by focusing on key flow regime components.

The negative verification mean error (ME) of the performance analysis indicates the model overall underestimates the fish abundance (Table 3). The maximum absolute verification error (Emax = 0.688 CPUE) indicates the model presents good performance in predicting high fish abundances values. This error represents less than 2% of the fish abundance peak of this dataset configuration (41.8 CPUE). The NS and r^2 performance indices also indicate the model can reproduce low and high fish abundances variation with good performance.

Table 3. Model performance analysis.

Dataset Configuration	Set	Nash-Sutcliffe coefficient NS	Mean error ME	Root mean square error RMSE	Coefficient of determination r^2	Maximum error Emax
1	Training	0.9999	0.0023	0.4328	0.9999	0.487
	Verification	0.9948	-1.3781	3.2898	0.9996	0.688
2	Training	0.9997	0.1281	0.8618	0.9997	0.773
	Verification	0.9794	-0.0465	0.5626	0.9800	0.277
3	Training	0.9997	0.0123	0.6837	0.9997	0.602
	Verification	0.9965	-1.4490	3.0455	0.9999	0.130

2.3.2 Functional Flow Regimes Analysis

We chose 6 functional flow regimes for analysis (Figure 11), which allow us to identify distinct fish abundance performances (orange bar) comparing the different functional flow regimes (blue line) and analyze the implications from the perspective of reservoirs' release decisions. The corresponding flow regime indices of each functional flow regime are detailed in Table 4.

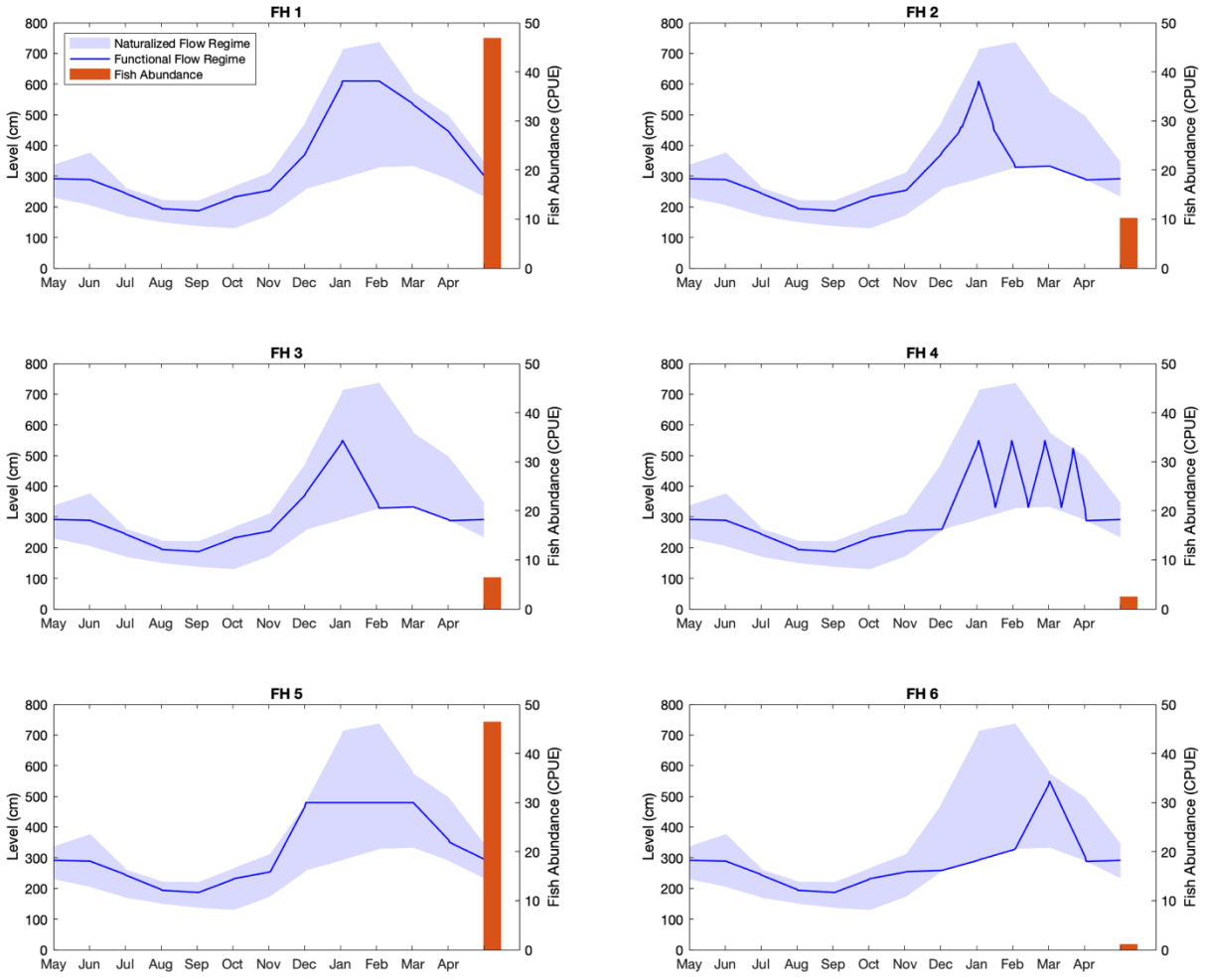

Figure 11. Functional flow regimes and the corresponding YoY fish abundance.

FH1 represents a scenario in which upstream reservoirs' release decisions are made to get close to the natural flow regime upper bound (favoring high flood magnitudes and duration, and low flood variability and delay). The longer the period of high-water levels, the higher is the possibility of juveniles to remain in the floodplain for feeding and be less susceptible to predation, improving conditions for the recruitment success. The result is a high YoY fish abundance response.

However, in terms of hydropower operation, high reservoir outflow releases in the rainy season to sustain fish recruitment may delay reservoir refilling, increasing the risk of future storage deficit and hydropower production. By utilizing the rating curve to convert water level into streamflow and comparing the other functional flows (FH2 to FH6) with FH1, it becomes possible to estimate the annual storage change upstream and assess how altering the characteristics of the released flow can mitigate the energy trade-off while still ensuring YoY fish abundance. The lower the water levels of a given FH compared to FH1, the lower the flow release and the more storage can be maintained upstream to either meet other water uses or improve drought protection in the next year.

In FH5, the reservoir release is reduced mostly in Jan-Feb to produce lower flood level magnitudes compared to FH1, while maintaining the flood duration, variability and delay. It shows that a high performance (YoY fish abundance) can still be obtained without outflow releases as significant as FH1. Once a minimum flood threshold level is reached, the floodplain connections already provide sufficient access to food and shelter for juvenile fish development, which warrants good results in fish abundance. From this magnitude on, there are diminishing returns to further change reservoir operation and recover the magnitude of the flow regime, considering fish abundance.

For upstream reservoir operation, this result is very important, as it means significant ecosystem restoration can still be obtained without necessarily using as much storage from upstream reservoirs as in FH1. The annual surplus of 24,782 hm^3 can be kept in upstream storage to maintain power generation later in the year and also help meeting other demands. Part of the Upper Paraná River Basin approximately 460,000 ha of irrigated crops could benefit from higher storage, especially during drought years.

In FH2, releases are still capable of reaching a similar high flood level magnitude as FH1, but with shorter durations, maintaining similar flood delay and variability. With less time to develop and access shelter and food in the floodplain, the juveniles return to the main channels more susceptible to predators, affecting recruitment. The YoY fish abundance response is then reduced by 78%, a significant performance loss. Despite this, the resulting fish abundance is above 10 CPUE, which is still relevant, considering that in 23 years of sampling collection just 5 years had YoY fish abundances above 10 CPUE. The 62,533 hm^3 in increased annual water storage upstream may be useful in drought years, when system storage is severely limited, and risk of near future energy and water deficits are high.

In FH3, the releases produce a flood magnitude slightly lower than FH2, but with similar total duration above the *FSD Low magnitude*. Although YoY fish abundance is further reduced from FH2, it may be another intermediate option, adequate for scenarios whose reservoir storage must be guaranteed to reduce future hydropower deficit risk (increase in 52,064 hm^3 upstream storage) but still producing relevant YoY fish abundance (above 6 CPUE).

FH4 represents a scenario with similar flood magnitude but higher variability and delay than FH3. Release decisions that produce such behavior in the floodplain should be avoided since the YoY fish abundance response is very low and the trade-offs for reservoir operation may be less beneficial than other scenarios. High water level variabilities increase the risk of predation and induce resorption of gonads, affecting spawning. The 44,384 hm^3 in increased annual water storage upstream is close to the FH3 result; however, the YoY fish abundance response is reduced, which indicates that similar water storage can be obtained managing timing and variability and with better YoY fish abundance response than the one showed in FH4.

Finally, in FH6 release decisions produce a moderate flood duration with a long delay. Delaying the flood in more than 140 days causes it to miss a critical time window for gonadal maturation and upstream migration. A too late flood resulted in the worst performance in fish abundance, and it should also be avoided. Instead, anticipating the same flow release in one or two months would produce better YoY fish response, as shown in FH2 and FH3.

Table 4. Flow regime indices of each functional flow regime.

FH	FSD High magnitude (days)	FSD Mid magnitude (days)	FSD Low magnitude (days)	Max Magnitude (cm)	Flood pulses (cycles)	Uninterrupted Flood duration (days)	Flood Delay (days)	DSD (days)	Inter-annual flood occurrence (years)	YoY Fish Abundance (CPUE)
1	32	35	43	610	1	110	71	96	0	46.7
2	1	12	17	610	1	30	76	96	0	10.3
3	0	2	30	550	1	32	75	96	0	6.5
4	0	3	45	550	4	18	81	96	0	2.6
5	0	0	100	480	1	100	58	96	0	46.0
6	0	2	23	550	1	25	140	96	0	1.2

2.4 Conclusion

The proposed methodology framework investigated how functional flow regimes can be generated, organized according to specific flow components, and have its performance measured in terms of fish response. Some specific conclusions are possible:

1. Different combinations of flow regime components bring different ecological response performance. While flow magnitude and duration are key contributors to performance for the ecological function modeled, there is a clear threshold above which performance gains are smaller;
2. The conclusion at (1) indicate the presence of diminishing marginal performance gains when designing an environmental flow, which are important when the tradeoffs between options are brought into flow allocation discussion among competing uses;
3. Although not always reaching the best response level, relevant YoY fish abundance can still be obtained when combining different flow regime components. This indicates that there is some flexibility in system operation. This flexibility should be explored, with the help of the results provided by the methods proposed here, in the preparation of more robust ecosystem restoration plans.
4. Some options should clearly be avoided, as their performance in terms of fish abundance is very low.

All the conclusions highlight that restoring flow regimes to improve ecosystem services is a water allocation exercise. Once several functional flows are designed, users will know how much water, when and under which variation pattern, is necessary to attain different levels of performance. This is the starting point to support water managers in exploring alternative reservoir operating schemes that perform well in releasing water towards YoY fish abundance relative to other system objectives. The proposed framework is flexible, which allows its application to other areas and ecological functions by changing the input hydrological time-series and adjusting the flow regime indices.

2.5 Appendix I. Naturalized flow regime estimation

A three-step procedure was adopted to generate the naturalized flow regime at the study area. First, the altered time-series of daily flow upstream (Porto Primavera and Rosana powerplants) were correlated with the respective altered time-series of daily level downstream (at Porto São Jose gauging station) with a Multiple Linear Regression (1). The resulting coefficient of determination (r^2) of 0.923 indicated that both independent variables can satisfactorily explain the level at Porto São José station (Eq. 1).

$$L_{PSJ} = 0.03709.Q_{PM} + 0.03217.Q_{ROS} - 6.9733 \quad \text{(Eq. 1)}$$

Where, L_{PSJ} is the level at Porto São José station (cm); Q_{PM} is the flow at Porto Primavera (m^3/s); and Q_{ROS} is the flow at Rosana (m^3/s).

Second, the relationship (1) was used to estimate the naturalized time-series of daily level downstream (at Porto São Jose gauging station), using as input the naturalized flow time-series upstream (Porto Primavera and Rosana powerplants) obtained from the Brazilian Independent System Operator – ONS (Agência Nacional de Águas (ANA), 2020), which reverts the flow regulation effects and evaporation losses of the reservoirs part of the hydropower system. As the relationship (1) includes levels at a maintained stage-discharge station, it is transferable across different naturalized flow input data. Finally, the estimated naturalized time-series of daily level downstream (at Porto São Jose station) was used to identify the range of the regime variability in an annual period (outliers were removed).

2.6 Appendix II. Flow regime indices analysis

Table 5 presents the resulting flow regime indices for each year of the observed level time-series at Porto São José Station with the corresponding observed floodplain YoY fish abundance.

Table 5. Flow regime indices calculated for the Paraná River target reach.

Flood Year (1)	FSD High magnitude (days)	FSD Mid magnitude (days)	FSD Low magnitude (days)	Max Magnitude (cm)	Flood pulses (cycles)	Uninterrupted Flood duration (days)	Flood Delay (days)	DSD (days)	Inter-annual flood occurrence (years)	YoY Fish Abundance(2) (CPUE)
1985	0	0	0	365	0	0	365	0	0	NA
1986	0	0	0	430	0	0	365	19	1	NA
1987	0	7	37	584	6	15	103	11	2	NA
1988	0	10	32	602	3	23	105	4	0	NA
1989	24	6	10	790	2	35	84	0	0	NA
1990	19	23	16	696	2	37	125	24	0	NA

1991	3	16	31	613	4	29	117	0	0	20.15
1992	16	6	71	664	6	44	42	0	0	41.82
1993	0	9	20	606	2	24	109	2	0	4.52
1994	14	8	13	652	2	26	104	1	0	NA
1995	0	0	2	476	1	2	161	6	0	NA
1996	28	10	8	853	1	46	103	12	0	NA
1997	2	9	41	618	4	22	151	0	0	NA
1998	0	7	39	598	12	13	0	0	0	NA
1999	0	0	4	508	1	4	175	3	0	0.00
2000	0	0	0	414	0	0	365	11	0	0.00
2001	0	0	12	530	3	9	138	92	1	1.00
2002	0	0	11	502	3	7	121	82	0	0.15
2003	0	0	3	481	1	3	199	48	0	0.20
2004	14	6	13	726	2	30	105	42	0	3.62
2005	0	0	20	512	7	8	81	37	0	0.41
2006	46	5	6	679	1	57	103	5	0	40.31
2007	0	0	10	497	2	9	178	20	0	0.91
2008	0	0	5	506	2	4	149	2	0	0.38
2009	40	32	31	741	5	75	16	28	0	46.42
2010	18	8	17	726	5	29	113	10	0	2.05
2011	0	0	4	487	1	4	120	6	0	0.08
2012	0	0	0	428	0	0	365	2	0	0.00
2013	0	0	0	402	0	0	365	23	1	0.00
2014	0	0	0	328	0	0	365	93	2	0.00
2015	2	6	18	637	3	12	91	92	3	18.80
2016	0	0	0	402	0	0	365	31	0	0.00
2017	0	0	4	473	1	4	110	76	1	0.08
2018	0	0	0	348	0	0	365	93	0	0.00

(1) the year number corresponds to the year the flood season begins; (2) NA = not available

Four years with unique features were observed in the dataset (2006, 2015, 2010, 1991). The year 2006 presented long duration for magnitude levels above 610 cm (*FSD High magnitude*) and small duration for low and intermediate flood magnitudes (*FSD Low magnitude* and *FSD Mid magnitude*). The other years presented the opposite behavior (higher low and intermediate magnitude durations).

The year 2015 showed high YoY fish abundance (above 15 CPUE) although not presenting significant flood durations in the three magnitude ranges (total of 26 days above the 450cm level). Two main aspects may have contributed to this particular result: (a) the number of previous years without flood (highest record), and (b) the flood duration in the Ivinhema tributary. The flood duration in the Ivinhema lasted 190 days during the 2015 flood season (the highest dataset record), from which 26 days were combined with a flood in the Paraná River. As it is difficult to separate the YoY fish abundance related just to the specific sub-system (fish tend to disperse through floodplain), the result may have suffered a predominant influence of the Ivinhema great flood in that year.

On the opposite side, the year 2010, although presenting considerable flood duration (43 days above the 450cm level), resulted in low YoY fish abundance (2.05 CPUE). The previous year's great flood (highest dataset register) may have influenced this result (the opposite case of the

year 2015) through factors and conditions not studied here. Finally, the year 1991 presented a high fish abundance although having a high flood delay.

2.7 Appendix III. Artificial Neural Network training procedure

Figure 12 depicts the Nested Leave-One-Out Cross-Validation procedure used for training and verifying the performance of the Fish-Flow Model. The dataset configurations between training (TS) and verification set (VS) composed an outer loop, and for each iteration n, the $VS_{(n)}$ set was saved, while $TS_{(n)}$ was trained in an inner loop by applying the leave-one-out (LOO) technique, which consisted in leaving one non-zero register (j) out for checking the error (validation set) and using the remaining ones for the training process. For each iteration j of the inner loop, training was ceased, and the weights recorded when the validation error stopped improving to prevent overfitting. Finally, the weights and biases (w and b) that resulted in the best performance among the inner loop iterations were applied to the correspondent verification set $VS_{(n)}$ in order to evaluate the performance of each configuration of the outer loop.

The ANN training procedure was based on feedforward backpropagating the error (Rumelhart et al., 1986) and subsequently adjusting the weights based on the delta rule (Widrow & Hoff, 1960). The momentum factor and dynamic learning rate were applied as accelerating methods (Vogl et al., 1988). The flowchart in Figure 13 depicts the training, validation and verification processes applied. To minimize the ANNs limitation in extrapolating the domain of the training set, registers with unique features were assigned to the training set (see Appendix II for further details).

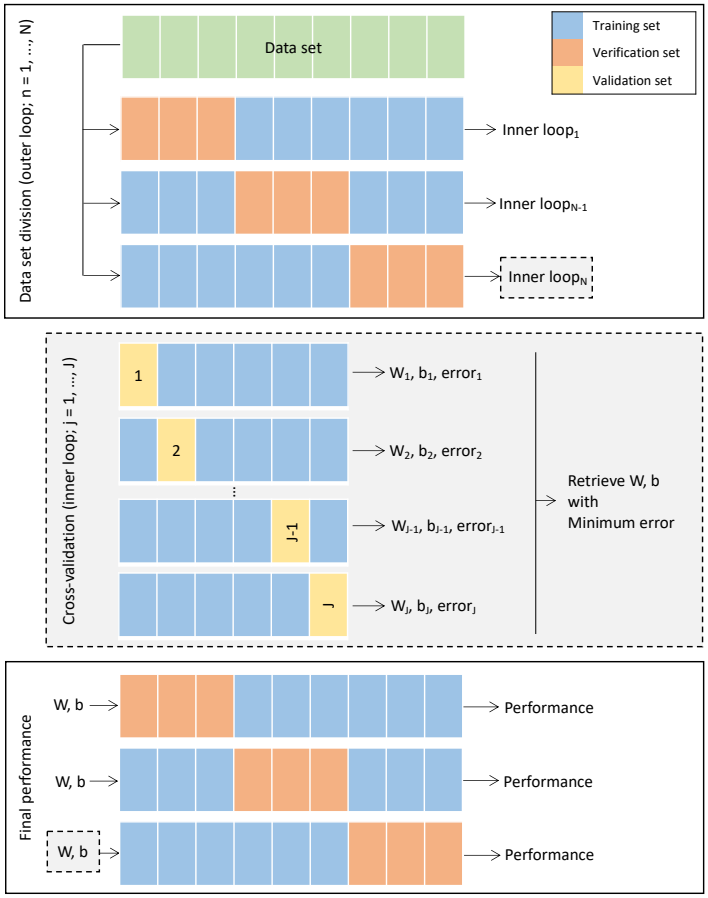

Figure 12. Nested Leave-One-Out Cross-Validation procedure.

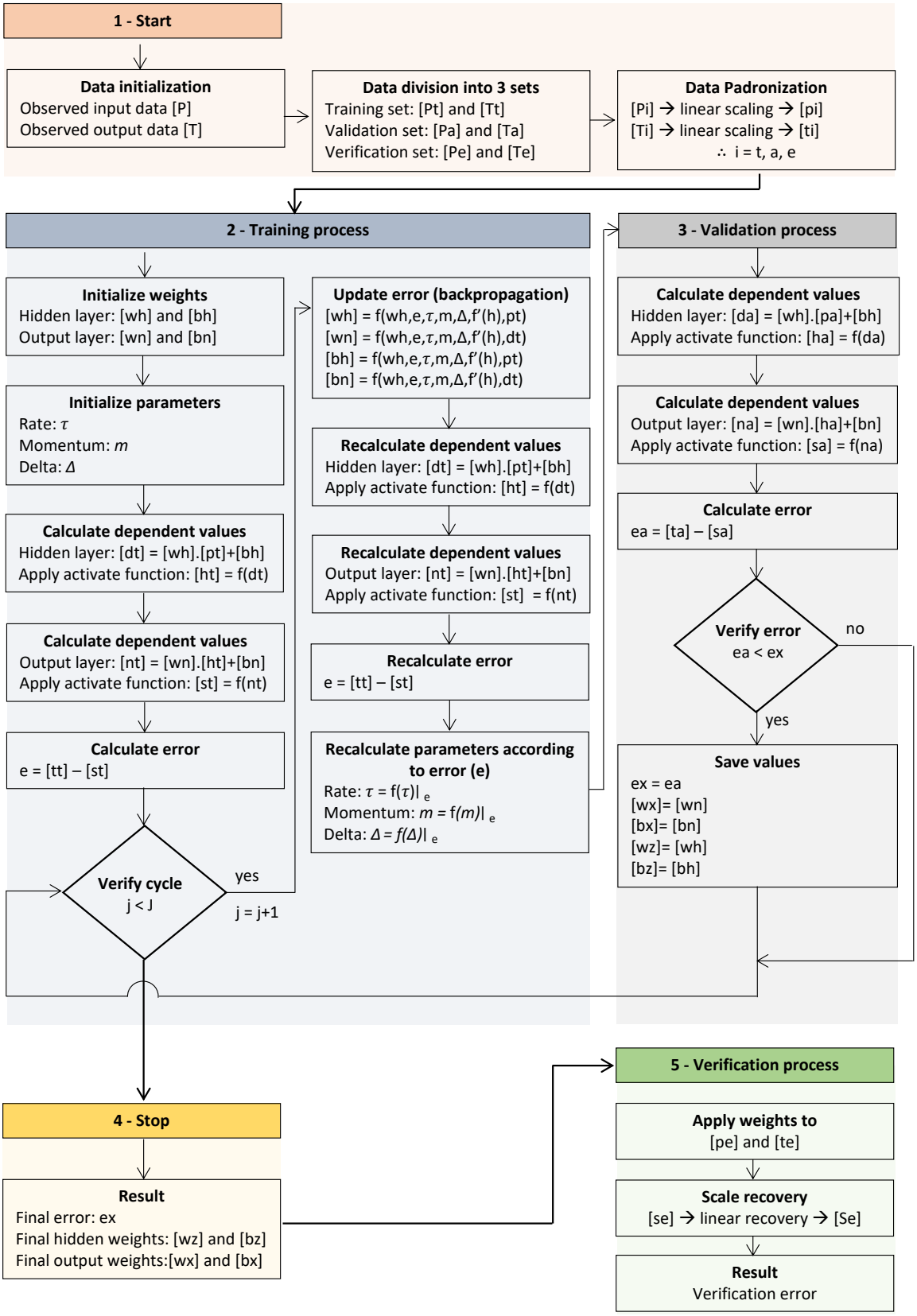

Figure 13. Flowchart of the Training, Validation and Verification Processes.

2.8 Appendix IV. Flow regime indices relevance

We checked the performance response of the model to each flow regime index as an indicative of its contribution to explain the observed fish abundance (Lek et al., 1996). The ANN model dataset was retrained leaving one input variable out at each simulation (Table 6).

Table 6. Average performance reduction analysis for each input variable removed.

Input variable removed	r^2	Performance reduction (%)	NS	Performance reduction (%)
none	0.993	-	0.990	-
FSD High magnitude	0.992	-0.1	0.941	-5.0
FSD Mid magnitude	0.843	-15.2	0.754	-23.9
FSD Low magnitude	0.913	-8.1	0.540	-45.5
Max Magnitude	0.992	-0.1	0.941	-5.0
Flood Pulses	0.712	-28.3	0.690	-30.3
Uninterrupted Flood Duration	0.992	-0.1	0.980	-1.0
Flood Delay	0.993	-0.1	0.906	-8.5
DSD	0.993	0.0	0.944	-4.6
Inter-annual Flood Occurrence	0.990	-0.3	-5.096	-614.7

The indices *FSD Low magnitude*, *FSD Mid magnitude*, and *Flood pulses* had high influence on the performance, indicating that the flood duration and its variability play an important role on the migratory fish recruitment. The *inter-annual flood occurrence* index must be analyzed with caution. Just one dataset register (year 2016) is characterized by having 3 previous years without flood, which may not be generalized for other events alike.

The high abundance of this year can have been influenced by other conditions not analyzed here that triggered high rates of fish reproduction despite not having the best flooding indices' conditions. The low performance reduction of the *DSD* index may indicate that low water level season may influence fish recruitment indirectly. One example is by allowing more vegetation growth during the dry season which provides increased food and shelter in the next flood season (Agostinho et al., 2000). However, the results do not allow a clear relationship to be defined.

2.9 Appendix V. Code and Programs Information

The codes in this study were designed by the author using the MATLAB (version R2021a) language.

2.10 References

Adamowski, J., & Karapataki, C. (2010). Comparison of Multivariate Regression and Artificial Neural Networks for Peak Urban Water-Demand Forecasting: Evaluation of Different ANN Learning Algorithms. Journal of Hydrologic Engineering, 15(10), 729–743. https://doi.org/10.1061/(ASCE)HE.1943-5584.0000245

Adams, L. E., Lund, J. R., Moyle, P. B., Quiñones, R. M., Herman, J. D., & O'Rear, T. A. (2017). Environmental hedging: A theory and method for reconciling reservoir operations for downstream ecology and water supply. Water Resources Research, 53(9), 7816–7831. https://doi.org/10.1002/2016WR020128

Agostinho, A. A., Thomaz, S. M., Minte-Vera, C. V., & Winemiller, K. O. (2000). Biodiversity in the high Paraná River flooplain. In Biodiversity in wetlands: assessment, function and conservation. Backhuys Publishers.

Agostinho, A. A., Pelicice, F. M., Petry, A. C., Gomes, L. C., & Júlio, H. F. (2007). Fish diversity in the upper Paraná River basin: habitats, fisheries, management and conservation. Aquatic Ecosystem Health & Management, 10(2), 174–186. https://doi.org/10.1080/14634980701341719

ANA. (2020a). Hidroweb. Retrieved February 1, 2020, from http://www.snirh.gov.br/hidroweb/apresentacao

ANA. (2020b). SAR - Sistema de acompanhamento de reservatórios. Retrieved from https://www.ana.gov.br/sar/

Arthington, A.H., Bunn, S. E., Poff, N. L., & Naiman, R. J. (2006). The challenge of providing environmental flow rules to sustain river ecosystems. Ecological Applications, 16(4), 8. https://doi.org/10.1890/1051-0761(2006)016[1311:TCOPEF]2.0.CO;2

Arthington, Angela H., Bhaduri, A., Bunn, S. E., Jackson, S. E., Tharme, R. E., Tickner, D., et al. (2018). The Brisbane Declaration and Global Action Agenda on Environmental Flows (2018). Frontiers in Environmental Science, 6. https://doi.org/10.3389/fenvs.2018.00045

CCEE. (2020). Hydroedit - apoio à leitura de arquivos. Retrieved December 10, 2020, from https://www.ccee.org.br/portal/faces/pages_publico/o-que-fazemos/como_ccee_atua/precos/deck_de_precos

Chen, W., & Olden, J. D. (2017). Designing flows to resolve human and environmental water needs in a dam-regulated river. Nature Communications, 8(1), 2158. https://doi.org/10.1038/s41467-017-02226-4

Comunello, É., E., S. F. E., Rocha, P. C., & Nanni, M. R. (2003). Dinâmica de inundação de áreas sazonalmente alagáveis na planície aluvial do Alto Rio Paraná: estudo preliminar. In SBRB (Ed.), SIMPÓSIO BRASILEIRO DE SENSORIAMENTO REMOTO (p. 470). Belo Horizonte. Retrieved from http://urlib.net/rep/ltid.inpe.br/sbsr/2002/11.14.17.20

Cooper, A. R., Infante, D. M., Daniel, W. M., Wehrly, K. E., Wang, L., & Brenden, T. O. (2017). Assessment of dam effects on streams and fish assemblages of the conterminous USA. Science of the Total Environment, 586, 879–889. https://doi.org/10.1016/j.scitotenv.2017.02.067

Crespo, D., Albiac, J., Kahil, T., Esteban, E., & Baccour, S. (2019). Tradeoffs between Water Uses and Environmental Flows: A Hydroeconomic Analysis in the Ebro Basin. Water Resources Management, 33(7), 2301–2317. https://doi.org/10.1007/s11269-019-02254-3

Fernandes, J. A., Irigoien, X., Goikoetxea, N., Lozano, J. A., Inza, I., Pérez, A., & Bode, A. (2010). Fish recruitment prediction, using robust supervised classification methods. Ecological Modelling, 221(2), 338–352. https://doi.org/10.1016/j.ecolmodel.2009.09.020

Freeman, M. C., Bowen, Z. H., Bovee, K. D., & Irwin, E. R. (2001). Flow and habitat effects on juvenile fish abundance in natural and altered flow regimes. Ecological Applications, 11(2), 631–631. https://doi.org/10.1890/1051-0761(2001)011[0179:FAHEOJ]2.0.CO;2

Grantham, T. E., Mount, J., Stein, E. D., & Yarnell, S. . (2020). Making the Most of Water for the Environment: A Functional Flows Approach for California's Rivers. San Francisco, CA, United States. Retrieved from https://www.ppic.org/wp-content/uploads/making-the-most-of-water-for-the-environment-a-functional-flows-approach-for-californias-rivers.pdf

Grill, G., Lehner, B., Lumsdon, A. E., MacDonald, G. K., Zarfl, C., & Reidy Liermann, C. (2015). An index-based framework for assessing patterns and trends in river fragmentation and flow regulation by global dams at multiple scales. Environmental Research Letters, 10(1), 015001. https://doi.org/10.1088/1748-9326/10/1/015001

Harwood, A., Johnson, S., Richter, B., Locke, A., Yu, X., & Tickner, D. (2017). Listen to the river: Lessons from a global review of environmental flow success stories. Woking, UK. Retrieved from https://www.wwf.org.uk/sites/default/files/2017-09/59054 Listen to the River Report download AMENDED.pdf

Holmlund, C. M., & Hammer, M. (1999). Ecosystem services generated by fish populations. Ecological Economics, 29(2), 253–268. https://doi.org/10.1016/S0921-8009(99)00015-4

Howard, J. K., Fesenmyer, K. A., Grantham, T. E., Viers, J. H., Ode, P. R., Moyle, P. B., et al. (2018). A freshwater conservation blueprint for California: prioritizing watersheds for freshwater biodiversity. Freshwater Science, 37(2), 417–431. https://doi.org/10.1086/697996

Hu, J. H., Tsai, W. P., Cheng, S. T., & Chang, F. J. (2020). Explore the relationship between fish community and environmental factors by machine learning techniques. Environmental Research, 184(1), 109262. https://doi.org/10.1016/j.envres.2020.109262

Joy, M. K., & Death, R. G. (2004). Predictive modelling and spatial mapping of freshwater fish and decapod assemblages using GIS and neural networks. Freshwater Biology, 49(8), 1036–1052. https://doi.org/10.1111/j.1365-2427.2004.01248.x

Lek, S., Belaud, A., Baran, P., Dimopoulos, I., & Delacoste, M. (1996). Role of some environmental variables in trout abundance models using neural networks. Aquatic Living Resources, 9(1), 23–29. https://doi.org/10.1051/alr:1996004

Li, F.-F., Wei, J.-H., Qiu, J., & Jiang, H. (2020). Determining the most effective flow rising process to stimulate fish spawning via reservoir operation. Journal of Hydrology, 582, 124490. https://doi.org/10.1016/j.jhydrol.2019.124490

Loures, R. C., & Pompeu, P. S. (2018). Long-term study of reservoir cascade in south-eastern Brazil reveals spatio-temporal gradient in fish assemblages. Marine and Freshwater Research, 69(12), 1983. https://doi.org/10.1071/MF18109

Marques, G. F., & Tilmant, A. (2018). Cost Distribution of Environmental Flow Demands in a Large-Scale Multireservoir System. Journal of Water Resources Planning and Management, 144(6), 04018024. https://doi.org/10.1061/(ASCE)WR.1943-5452.0000936

McKay, S. K., Linkov, I., Fischeinch, J. C., Miller, S. J., & Valverde, L. J. jr. (2012). Ecosystem Restoration Objectives and Metrics. U.S. https://doi.org/ERDC TN-EMRRP-EBA-16

Moyle, P. B., Katz, J. V. E., & Quiñones, R. M. (2011). Rapid decline of California's native inland fishes: A status assessment. Biological Conservation, 144(10), 2414–2423. https://doi.org/10.1016/j.biocon.2011.06.002

Olden, J. D., & Poff, N. L. (2003). Redundancy and the choice of hydrologic indices for characterizing streamflow regimes. River Research and Applications, 19(2), 101–121. https://doi.org/10.1002/rra.700

Oliveira, A. G., Suzuki, H. I., Gomes, L. C., & Agostinho, A. A. (2015). Interspecific variation in migratory fish recruitment in the Upper Paraná River: effects of the duration and timing of floods. Environmental Biology of Fishes, 98(5), 1327–1337. https://doi.org/10.1007/s10641-014-0361-5

Oliveira, Anielly Galego de, Lopes, T. M., Angulo-Valencia, M. A., Dias, R. M., Suzuki, H. I., Costa, I. C. B., & Agostinho, A. A. (2020). Relationship of Freshwater Fish Recruitment With Distinct Reproductive Strategies and Flood Attributes: A Long-Term View in the Upper Paraná River Floodplain. Frontiers in Environmental Science, 8. https://doi.org/10.3389/fenvs.2020.577181

Ota, R. R., Deprá, G. de C., Graça, W. J. da, & Pavanelli, C. S. (2018). Peixes da planície de inundação do alto rio Paraná e áreas adjacentes: revised, annotated and updated. Neotropical Ichthyology, 16(2). https://doi.org/10.1590/1982-0224-20170094

Palmer, M., & Ruhi, A. (2019). Linkages between flow regime, biota, and ecosystem processes: Implications for river restoration. Science, 365(6459), eaaw2087. https://doi.org/10.1126/science.aaw2087

Piffady, J., Souchon, Y., Capra, H., & Parent, E. (2010). Quantifying the effects of temperature and flow regime on the abundance of 0+ cyprinids in the upper River Rhone using Bayesian hierarchical modelling. Freshwater Biology, 55(11), 2359–2374. https://doi.org/10.1111/j.1365-2427.2010.02453.x

Poff, N., Tharme, R., & Arthington, A. (2017). Evolution of Environmental Flows Assessment Science, Principles, and Methodologies. In Water for the Environment (pp. 203–236). https://doi.org/10.1016/B978-0-12-803907-6.00011-5

Poff, N. L., Allan, J. D., Bain, M. B., Karr, J. R., Prestegaard, K. L., Richter, B. D., et al. (1997). The Natural Flow Regime. BioScience, 47(11), 769–784. https://doi.org/10.2307/1313099

Poff, N. L., Tharme, R. E., & Arthington, A. H. (2017). Evolution of Environmental Flows Assessment Science, Principles, and Methodologies. In Water for the Environment (pp. 203–236). Elsevier. https://doi.org/10.1016/B978-0-12-803907-6.00011-5

Pringle, C. M., Freeman, M. C., & Freeman, B. J. (2000). Regional Effects of Hydrologic Alterations on Riverine Macrobiota in the New World: Tropical–Temperate Comparisons. BioScience, 50(9), 807:823. https://doi.org/https://doi.org/10.1641/0006-3568(2000)050[0807:REOHAO]2.0.CO;2

Quesne, L., Kendy, E., & Weston, D. (2010). The Implementation Challenge - Taking Stock of Government Policies to Protect and Restore Environmental Flows. UK. Retrieved from http://www.conservationgateway.org/Documents/Global flows report final LowRes.pdf

Rumelhart, D. E., Hinton, G. E., & Williams, R. J. (1986). Learning representations by back-propagating errors. Nature, 323(6088), 533–536. https://doi.org/10.1038/323533a0

Sadiq, R., Rodriguez, M. J., & Mian, H. R. (2019). Empirical Models to Predict Disinfection By-Products (DBPs) in Drinking Water: An Updated Review. In Encyclopedia of Environmental Health (pp. 324–338). Elsevier. https://doi.org/10.1016/B978-0-12-409548-9.11193-5

Suen, J.-P., & Eheart, J. W. (2006). Reservoir management to balance ecosystem and human needs: Incorporating the paradigm of the ecological flow regime. Water Resources Research, 42(3). https://doi.org/10.1029/2005WR004314

Suzuki, H., Agostinho, A., Bailly, D., Gimenes, M., Júlio-Junior, H., & Gomes, L. (2009). Inter-annual variations in the abundance of young-of-the-year of migratory fishes in the Upper Paraná River floodplain: relations with hydrographic attributes. Brazilian Journal of Biology, 69(2 suppl), 649–660. https://doi.org/10.1590/s1519-69842009000300019

Tharme, R. E. (2003). A global perspective on environmental flow assessment: emerging trends in the development and application of environmental flow methodologies for rivers. River Research and Applications, 19(5–6), 397–441. https://doi.org/10.1002/rra.736

Tilmant, A., Arjoon, D., & Marques, G. F. (2014). Economic Value of Storage in Multireservoir Systems. Journal of Water Resources Planning and Management, 140(3), 375–383. https://doi.org/10.1061/(ASCE)WR.1943-5452.0000335

Tonkin, Z., Yen, J., Lyon, J., Kitchingman, A., Koehn, J. D., Koster, W. M., et al. (2021). Linking flow attributes to recruitment to inform water management for an Australian freshwater fish with an equilibrium life-history strategy. Science of the Total Environment, 752, 141863. https://doi.org/10.1016/j.scitotenv.2020.141863

Vogl, T. P., Mangis, J. K., Rigler, A. K., Zink, W. T., & Alkon, D. L. (1988). Accelerating the convergence of the back-propagation method. Biological Cybernetics, 59(4–5), 257–263. https://doi.org/10.1007/BF00332914

Wang, C., Jiang, Z., Zhou, L., Dai, B., & Song, Z. (2019). A functional group approach reveals important fish recruitments driven by flood pulses in floodplain ecosystem. Ecological Indicators, 99(September 2018), 130–139. https://doi.org/10.1016/j.ecolind.2018.12.024

Whitfield, A. K., & Elliott, M. (2002). Fishes as indicators of environmental and ecological changes within estuaries: a review of progress and some suggestions for the future. Journal of Fish Biology, 61(sa), 229–250. https://doi.org/10.1111/j.1095-8649.2002.tb01773.x

Widrow, B., & Hoff, M. E. (1960). Adaptive switching circuits. IRE Wescon Convention Record, 8(4), 96–104.

Wild, T. B., Reed, P. M., Loucks, D. P., Mallen-Cooper, M., & Jensen, E. D. (2019). Balancing Hydropower Development and Ecological Impacts in the Mekong: Tradeoffs for Sambor Mega Dam. Journal of Water Resources Planning and Management, 145(2), 05018019. https://doi.org/10.1061/(ASCE)WR.1943-5452.0001036

Wong, T.-T. (2015). Performance evaluation of classification algorithms by k-fold and leave-one-out cross validation. Pattern Recognition, 48(9), 2839–2846. https://doi.org/10.1016/j.patcog.2015.03.009

Yarnell, S. M., Petts, G. E., Schmidt, J. C., Whipple, A. A., Beller, E. E., Dahm, C. N., et al.

(2015). Functional Flows in Modified Riverscapes: Hydrographs, Habitats and Opportunities. BioScience, 65(10), 963–972. https://doi.org/10.1093/biosci/biv102

CHAPTER 3

Modeling Large-scale Hydropower Systems with Stochastic Dual Dynamic Programming – Application to the Paraná River Basin

3.1 Introduction

While energy generation and prices are more predictable in energy matrices composed mainly of thermopower plants, in hydropower-dominant matrices, future hydrological uncertainties impose greater complexity and risk on energy generation, resulting in more variable energy prices. Although hydropower plants have no direct operating costs related to fuel expenses, the decision to release water today affects the availability of resources for the future (reservoir storage) and, consequently, the benefits and costs of the system (e.g., deficit costs, thermal complementation costs) (Pereira & Pinto, 1985).

Planning hydropower generation under hydrological uncertainties requires the implementation of optimization approaches. The objective is to determine release decisions that minimize operating costs (or maximize the benefits) throughout the planning horizon, while constrained by operational constraints. The Direct Policy Search (DPS) and the Stochastic Dual Dynamic Programming (SDDP) are two policy formulations that have the advantage of handling large-scale multi-reservoir systems. While the former operates in the policy space by parameterizing the operating policy within a family of functions (e.g., radial basis functions), the Stochastic Dual Dynamic Programming (SDDP) operates in the value space by providing piecewise benefit-to-go functions (Giuliani et al., 2021).

In countries like Brazil and the Nordic countries, where hydroelectricity represents the main energy source, the stochastic dual dynamic programming (SDDP) technique is implemented to address the time dependency and the stochasticity of the inflows (CEPEL, 2012; Gjelsvik et al., 2010). More specifically, in the case of Brazil, various studies have also proposed alternatives, adaptations, and simplifications in modeling the hydropower operation, with the majority utilizing non-linear optimization techniques. For example, Barros et al. (2003) developed a non-linear model to support the management and operation of the Brazilian hydrothermal system. Zambon et al. (2012) presented a non-linear model capable of handling different types of constraints, such as interbasin water transfers, water supply, and environmental requirements.

Hydrolab is another decision support software developed for planning and programming the operation of the National Interconnected System (Cicogna, 2003; Cicogna & Filho, 2006). It uses deterministic non-linear programming to determine the operation of individual hydrothermal plants, while the inflow forecast is generated stochastically by combining artificial neural network and fuzzy models. Non-linear algorithms have also been applied to include other constraints/conditions in the system planning operation. For example, Pereira (2006) incorporated temporal hydropower plant shutdowns for preventive maintenance, Santos (2015) focused on planning short-term operations constrained by security conditions of transmission lines, transformers, and generators, and Hidalgo et al. (2020) assessed the impact of future climate scenarios.

Despite the availability of different alternatives, the Stochastic Dual Dynamic Programming (SDDP) approach was chosen to model the operation of the hydropower system of the study area. This approach was selected due to its ability to optimize large-scale water resource systems while explicitly considering uncertainty. Stochastic approaches can capture the uncertain nature of the reservoir operating problem without resorting to certainty equivalence assumptions, i.e., when a decision policy is defined by putting the uncertainty equal to its expected value given the observation (Van de Water & Willems, 1981).

Additionally, this method enables the assessment of marginal water values at each stage (e.g., the value of water storage), providing valuable insights for hydroeconomic analysis (Rougé & Tilmant, 2016). The approach is also not dependent on specific predefined functions classes and policy architecture (Giuliani et al., 2021), allowing a broad operation range to be explored. The model framework followed the structure presented in Tilmant & Kelman (2007), Tilmant et al. (2008a) and latter in Goor et al. (2011) and it was adapted to fit the local conditions and to model the individual reservoirs' release decisions of the Paraná River Basin for long-term planning.

This chapter is organized by first providing an overview of the Brazilian Integrated Power System and explaining the concepts of the SDP (Stochastic Dynamic Programming) and SDDP (Stochastic Dual Dynamic Programming) approaches. It then applies the SDDP approach to the Paraná River Basin, demonstrating the input data and configuration assumptions. Finally, the simulation results are presented by comparing them to the observed data to assess the model's performance and its suitability in representing the operation of the national power system. Further inclusion of other objectives in the optimization approach is described in the following chapters of this dissertation (chapter 5).

3.2 An overview of the Brazilian Integrated Power System

The Brazilian power system is organized in 4 interconnected submarkets: North (N), Northeast (NE), South (S) and Southeast/Midwest (SE/CO), Figure 14. The interconnected system enables the submarkets to exchange energy within the limits imposed by the transmission grid, exploring the hydrological complementarity from the diverse hydrological regimes across the country to reduce energy production cost (ONS, 2020). In 2021, about 60.2% of the installed power generation was derived from hydropower plants, 16% from non-renewable fossil fuel based thermal plants (gas, coal, oil), 8.8% biomass 11.4% from wind power, 2.6% solar sources and 1.1% nuclear (EPE, 2022).

Figure 14. Interconnect submarkets of the Brazilian power system. Source: (ONS, 2023).

The operation planning of the Brazilian Integrated System is divided in three main horizons - long-term, short-term and daily schedule - each applying models representing the system with

different degrees of detail. In the long-term planning, the system is represented by subsystems (or submarkets) of aggregated power plants (reservoirs of equivalent energy). The monthly thermal and hydro energy generation cost (composed mainly of fuel costs for thermopower generation and penalties for energy deficit) is minimized for a five-year planning horizon using an optimization approach based on Stochastic Dual Dynamic Programming (Eletrobras, 2020).

Hydrological conditions and energy demand derive the optimum point between the current water use and the future storage in order to minimize the use of very expensive thermopower generation or even fail the load supply. As a result, the model builds a cost function over time, while the constraints' multipliers (lambdas) represent the Marginal Operating Costs (CMO) for each stage, load level and subsystem (Eletrobras, 2020).

In the sequence, the short-term planning discretizes the one-year planning in weekly time steps for the first month and monthly time steps for the remaining ones with the objective of determining the individual hydro and thermal power plants generation. By discretizing the subsystems' individual power plants, the release decisions are again optimized in order to minimize the costs against the necessity of switching on thermopower plants (Eletrobras, 2020). The last stage considers the cost function obtained in the long-term planning as input to calculate the cost function for the weekly stages. Daily and hourly schedules are calculated in sequence.

The NEWAVE model (for the long-term planning) and the DECOMP (for the short-term planning) are the official tools applied by the ONS for launching the monthly releases policies of the system and by the CCEE for determining the energy price practiced in the spot market. The stochastic inflows are produced by the GEVAZP model (Generation of Synthetic Series of Energies and Periodic Flow). Finally, the DESSEM model determines the daily schedule of the operation and has being validated by ONS and CCEE for official use as of January 2020, to establish the hourly price of energy in Brazil (Eletrobras, 2020).

3.3 Methodology

3.3.1 Stochastic Dynamic Programming

To solve the hydropower operation problem with the Stochastic Dynamic Programming (SDP) method, the total planning horizon T is divided in stages *t,* and release decisions r_t are made at each stage to maximize current benefits f_t (or minimize the costs) in addition to the expected benefits from future operation (from t to the end of the planning period T). The expected benefits are represented by the recursive benefit-to-go function F_{t+1} [Eq. (1)].

$$F_t(s_t, q_t) = E_{h(t)}[max\{f_t(s_t, q_t, r_t) + F_{t+1}(s_{t+1}, q_{t+1})\}] \quad (1)$$

constrained by:

$$r_t = s_t + q_t - e_t - s_{t+1} \quad (2)$$

$$\underline{s}_{t+1} \leq s_{t+1} \leq \overline{s}_{t+1} \quad (3)$$

$$\underline{r}_t \leq r_t \leq \overline{r}_t \quad (4)$$

where t is the time index; S_t is the storage for the stage t; q_t is the inflow for the stage t; and r_t is the release for the stage t, E is the expectation operator to observe hydrological condition given the previous hydrological states.

The correlation between successive inflows is usually assumed to be governed by a Markov chain, which represents the hydrologic uncertainty by encoding the temporal persistence between successive flows into flow transition probabilities. Assuming that the continuous random variables q_{t-1} can be approximated by a discrete random variable q_{t-1} [Eq. (5)], the expectation operator E of equation (1) can be substituted by the conditional probabilities $P(q_t|q_{t-1})$ [Eq. (6)].

$$P(q_t|q_{t-1}, q_{t-2}, \dots, q_1) \cong P(q_t|q_{t-1}) \tag{5}$$

$$F_t(s_t, q_{t-1}) = \max_{r_t} \{f_t(s_t, q_{t-1}, r_t) + \sum_{q_{t-1}} P(q_t|q_{t-1}).F_{t+1}(s_{t+1}, q_t)\} \tag{6}$$

In the Stochastic Dynamic Programming method, solutions at each grid point are obtained by discretizing the state variables, such as reservoir storage and inflow (Figure 15). The disadvantage of the discrete approach is that the computational effort increases exponentially with the number of reservoirs. For example, by assuming k state variables, both discretized in N values, and J reservoirs, the number of possible combinations for each grid point is represented by $(N^K)^J$. For two state variables (inflow and storage), both discretized in 20 levels and 3 reservoirs, it results in 64 million combinations.

To address the dimensionality issue, Pereira & Pinto (1985) proposed the Stochastic Dual Dynamic Programming (SDDP) as an extension of the traditional stochastic dynamic programming (SDP) that is not affected by the curse of dimensionality, making it suitable for solving larger problems while considering stochastic state variables.

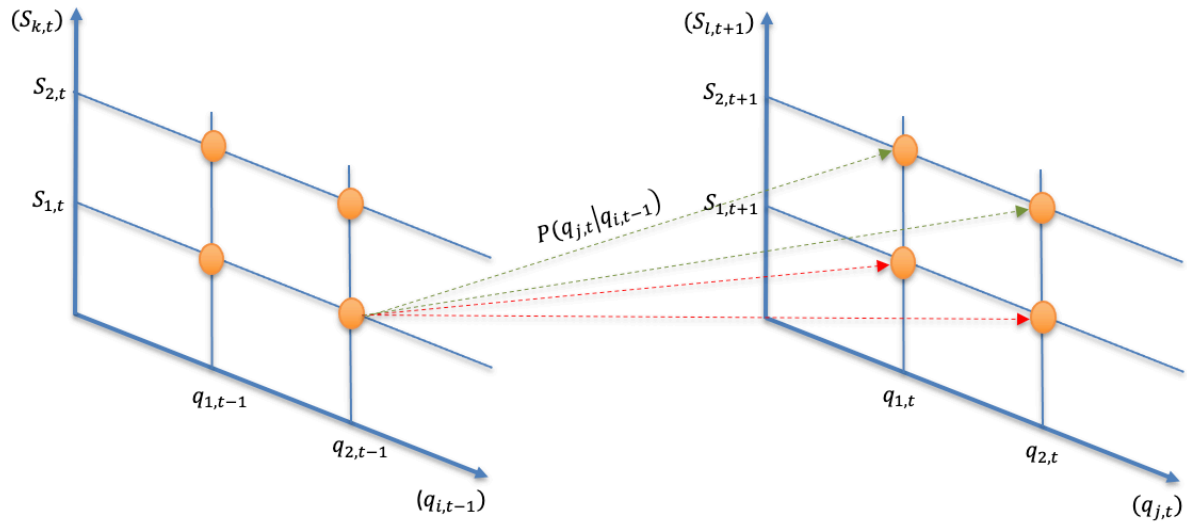

Figure 15. Representation of the state-domain discretization and recursive equation application.

3.3.2 Stochastic Dual Dynamic Programming (SDDP)

The stochastic dual dynamic programming (SDDP) method assumes that the operation of reservoirs typically does not span the entire state-space domain. Instead, the variation in reservoir storage is usually confined to a smaller range, which is the typical/historical operational variability (Figure 16).

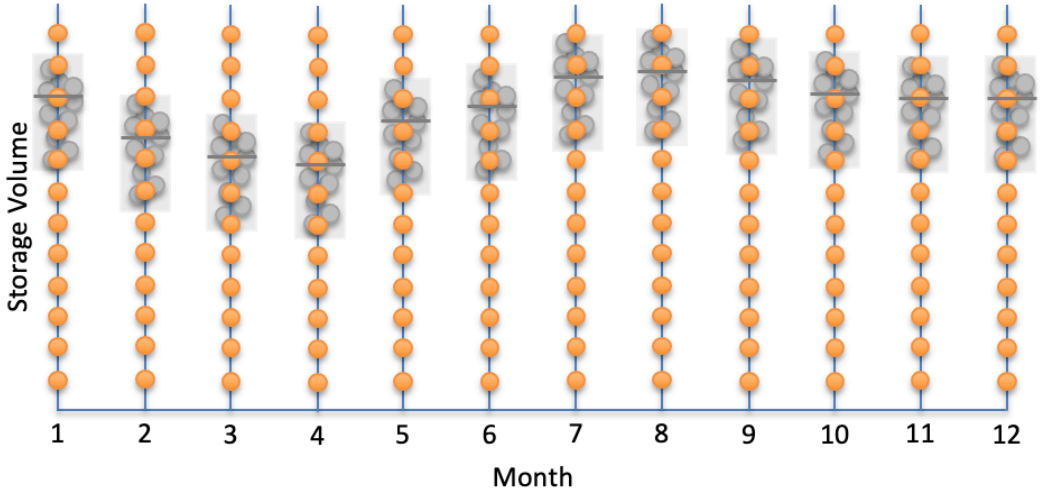

Figure 16. Entire domain (orange) versus operational domain (gray).

Hence, the SDDP method does not aim to calculate F_{t+1} for the entire discrete state domain. Instead, it builds a locally accurate approximation of F_{t+1} using piecewise linear segments (Figure 17). The linear segments are built as a function of the storage s_t and the inflow q_t utilizing domain sample points [Eq. (7)], through the application of decomposition techniques such as Benders and lagrangian decomposition, as described in Boschetti & Maniezzo (2009). The resulting hyperplane provides an outer approximation of the benefit-to-go function, while the computational effort is reduced since a limited number of values for the state variables (points) are now sufficient to provide an approximation of F_{t+1}.

$$\mathrm{F_{t+1}} \leq \alpha_{t+1}^{l} . s_{t+1} + \gamma_{t+1}^{l} . q_t + \beta_{t+1}^{l} \qquad l = 1, \ldots, L \tag{7}$$

where the index l represents the cut segments.

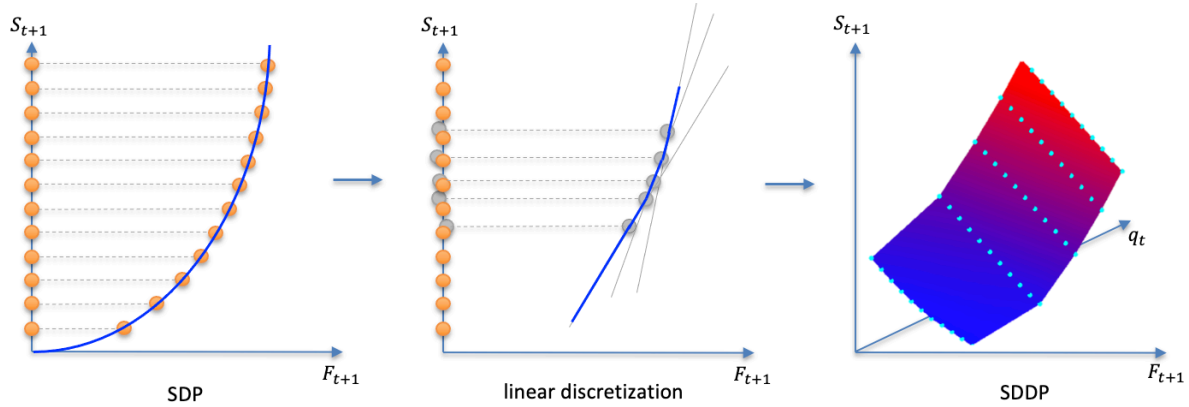

Figure 17. Representation of the benefit-to-go function $\mathrm{F_{t+1}}$ hyperplane creation.

The reformulation of the problem as a linear function allows for implementation of linear optimization methods to find the optimal release decision at each stage of the planning horizon. While the SDP method requires to calculate the combination of the current s_t and the future storages s_{t+1} for each grid point of the space-domain before moving to the next stage, the SDDP method obtains the optimal combination $[s_t, s_{t+1}]$ by linear optimization. At each stage, storage values s_t are sampled and the optimal future storage s_{t+1} for the corresponding sample point s_t is obtained by linear optimization. In the next stage, the process repeats, by sampling new

storage values s_t and obtaining the optimal s_{t+1} as the result of the linear optimization (Figure 18).

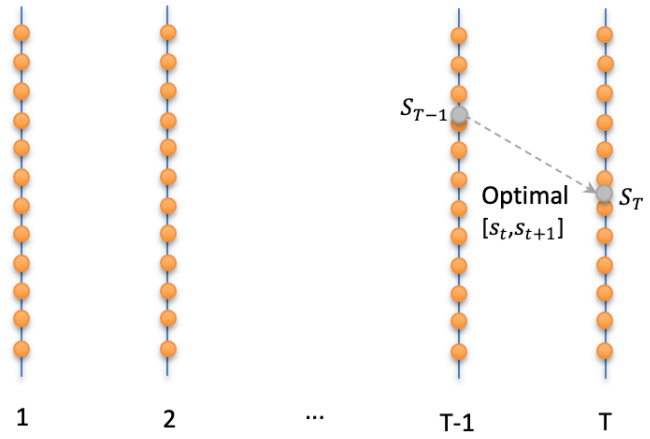

Figure 18. Representation of the result of the one stage linear optimization.

Since the accuracy of the approximation increases with the increasing number of linear segments, the SDDP method primes to gradually increase the number of linear segments until the accuracy reaches an accepted tolerance. This process iterates between two phases: forward simulation and backward optimization. The backward optimization phase focuses on constructing the cuts (linear segments) at each stage t, initially using a certain number of sample points. The generated cuts are then evaluated to determine if the approximation they provide is statistically acceptable. If the approximation is not acceptable, a new iteration begins, and a new backward optimization phase is implemented with a larger sample size, which includes the points from the last simulation.

3.3.3 Hydro-System Representation

Figure 19 depicts an example of a Hydro-System composed by multi reservoirs connected in series and/or in parallel. The connectivity matrix C^R represents the interactions between reservoirs, indicating whether water is being received (+1) or released (-1). The size of the matrix corresponds to the number of modeled reservoirs (J x J). The mass balance equation that integrates all reservoirs is them represented by [Eq. (8)], while the variables are represented by vectors of size J.

$$s_{t+1} = s_t + q_t - C^R(r_t + l_t) - e_t \tag{8}$$

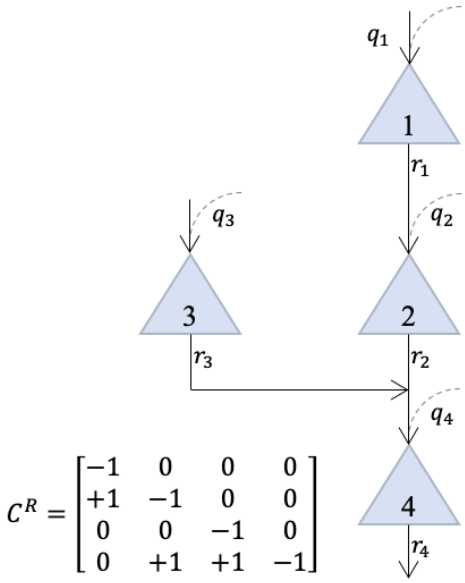

Figure 19. Hydro-system representation.

3.3.4 Hydrologic state variable

To implement linear optimization methods for solving each stage of the SDDP problem, all portions of equation (1), including the immediate benefit equation (f_t) and the inflows generation (q_t), must be analytically represented by a linear and differentiable equation.

To avoid the discretization of the hydrologic state variable, and to further reduce the computational effort required to solve the recursive equation (6), the natural reservoirs inflows q_t are estimated at each node of the hydro-system by an analytical build-in multi-site periodic autoregressive model of order p (MPAR(p)), which is linear and differentiable (Quentin Goor, 2010).

The hydrologic state variable is typically a vector of p previous flows q_{t-1}, q_{t-2}, q_{t-p}, which are then used to generate q_t using a built-in periodic autoregressive model MPAR(p) with cross-correlated residuals. Equation (9) represents the periodic process modelled by an autoregressive model of order 1. See appendix I for further information.

$$q_t = \mu_{q,t} + \phi_t . \frac{\sigma_{q,t}}{\sigma_{q,t-1}} . \left(q_{t-1} - \mu_{q,t-1}\right) + \sigma_{q,t} . \epsilon_t \tag{9}$$

where:

$\mu_{q,t}$ is the vector of the periodic mean of the current period reservoir inflows q_t
$\sigma_{q,t}$ is the vector of the standard deviation of the current period reservoir inflows q_t
ϕ_t is the vector of periodic autoregressive parameter of order 1
ϵ_t is a time independent (but spatially correlated) stochastic noise of zero mean and variance $\sigma^2_{\epsilon,t}$

3.3.5 Hydropower Production

The power generated by a hydropower plant depends on the product of the turbined outflow r_t and the net head h on the turbine [Eq. (10)].

$$P_t = r_t.h(s_t, s_{t+1}).\gamma.\eta(s_t, s_{t+1}, r_t) \quad (10)$$

where P_t is the power generated [W], the net head h on turbines [m] is a function of the average storage (s_t, s_{t+1}) during time period t; η is the turbines/generators efficiency as a function of the average head and the turbining during period t; and the γ is the specific weight of water [N/m^3].

As the production of hydroelectricity is a nonlinear function of the head (storage) and release variables, Quentin Goor (2010) presented a methodology that removes the nonconvexity by constructing a piecewise linear approximation of the true hydropower production function through convex hulls [Eq. (11)], allowing to be implemented in the one-stage optimization problem.

$$\widehat{P_t} \leq \varphi^h.\frac{s_{t+1} + s_t}{2} + \omega^h.r_t + \delta^h \quad \forall \quad h = 1, \dots, H \quad (11)$$

where H is the number of linear approximations of the true hydropower functions, that provide upper bounds to the true functions; $\widehat{P_t}$ is the approximated hydropower generated during period t and $\varphi^h, \omega^h, \delta^h$ are the parameters of the hyperplanes h.

To calculate the hyperplanes parameters $\varphi^h, \omega^h, \delta^h$, the feasible domain of the storage s_t and the release r_t of each hydropower station is first discretized and the true hydropower function $P(s_t, r_t)$ is calculated at each grid point. Then, $\widehat{P_t}(s_t, r_t)$ is estimated through a convex hull approximation by piecewise linear functions of the storage and turbining. The power production is limited by the installed capacity P_{max} of the hydropower plant [Eq. (12)].

$$\widehat{P_t} \leq P_{max} \quad (12)$$

3.3.6 Benefit equation

When dealing with hydropower multi-reservoirs' operation, a typical benefit function f_t includes the benefits of energy production minus the operation and maintenance costs (net revenue) [Eq. (13)].

$$HP_t = \tau_t \sum_{j=1}^{J} (\pi_t\ (j) - \theta\quad (j)).\rho(j).\widehat{P_t}(j) \quad (13)$$

where τ_t is the number of hours in period t; π_t is the energy price [\$/Wh]; θ is the operation and maintenance cost of hydropower plants [\$/Wh]; $\rho.\widehat{P_t}$ is the power generated by the hydropower plants during period t, and j is the reservoir index.

Penalties for not meeting operational and/or institutional constraints are usually included, resulting in the final benefit function f_t [Eq. (14)].

$$f_t(s_t, q_t, r_t) = HP_t - \zeta_t.z_t \quad (14)$$

where ζ_t is the penalty cost [\$/unit of deficit or surplus]; and z_t is the slack variables with the violations of operational constraints (e.g, energy deficit, environmental flows, etc).

3.3.7 One-stage optimization

3.3.7.1 Lagrange Multiplier method

The Lagrange Multiplier method is a calculus-based approach used to find optimal solutions of constrained optimization problems. It allows to translate the original constrained optimization problem into an ordinary system of simultaneous equations by introducing an extra variable λ. By applying partial derivatives, we can then determine the optimal solutions. Considering an example where we want to maximize y [Eq. (15)], which is constraint by g [Eq. (16)].

$$y = f(x_1, x_2, \dots, x_n) \tag{15}$$

$$g(x_1, x_2, \dots, x_n) = b \tag{16}$$

The lagrangian function combines the constraints equations with the objective function [Eq. (17)]. When constraints are not binding ($\lambda = 0$), so constraints can be ignored, or constraints are biding ($\lambda \neq 0$) and the constraint ($g(X) - b = 0$) is satisfied, Z and y are equivalent.

$$Z(x_1, x_2, \dots, x_n, \lambda) = f(x_1, x_2, \dots, x_n) + \lambda.[g(x_1, x_2, \dots, x_n) - b] \tag{17}$$

The objective function is maximized (or minimized) when each of its partial derivatives with respect to each unknown variable is equal to zero [Eq. (18)]. Setting the partial derivative with respect to λ equal to zero gives us the original constraint back [Eq. (19)]. Thus, the optimal condition is obtained by $\partial Z(x_i, \lambda) = 0$.

$$\frac{\partial Z}{\partial x_i} = \frac{\partial f}{\partial x_i} + \lambda \frac{\partial g}{\partial x_i} = 0 \qquad \mathrm{i} = 1,2,\dots,\mathrm{n} \tag{18}$$

$$\frac{\partial Z}{\partial \lambda} = g(x_1, x_2, \dots, x_n) - b = 0 \tag{19}$$

By manipulating equation (18), we can find the constraint multiplier λ, which represents the marginal value (additional benefit) from relaxing the constraint $g(X)$.

$$\lambda = -\frac{\partial f}{\partial g} \tag{20}$$

In the case of inequality constraints [Eq. (21)], the simple condition $\partial Z(x_i, \lambda) = 0$ is not anymore sufficient to guarantee a solution. However, the optimum might occur at a boundary. If the constraints are biding, besides Eq. (19), we must include the constraint multiplier λ with the opposite condition [Eq. (22)].

$$g(x_1, x_2, \dots, x_n) \geq b \tag{21}$$

$$\lambda \leq 0 \tag{22}$$

3.3.7.2 One stage decomposition representation

By representing the components f_t and F_{t+1} of Eq. (6) by their linear functions: [Eq. (14)] for f_t and [Eq. (7)] for F_{t+1}; and introducing the constraints of both components f_t and F_{t+1} and their corresponding Lagrange multipliers in the same equation, the one-stage function becomes equation (23).

$$Z(s_t, q_{t-1}, \lambda_{w,t}, \lambda_{HP,t}) = (HP_t - \zeta_t . z_t) + (\alpha_{t+1} . s_{t+1} + \gamma_{t+1} . q_t + \beta_{t+1}) + \lambda_{w,t} . (s_{t+1} - s_t - q_t + C^R(r_t + l_t) + e_t) + \lambda^h_{HP,t} . (\widehat{P_t} - \varphi^h . \frac{s_{t+1} + s_t}{2} - \omega^h . r_t - \delta^h) \quad (23)$$

Table 7. Constraints and lagrange multipliers of the functional equation in the analytical form.

Constraints	Lagrange multipliers
$s_{t+1} = s_t + q_t - C^R(r_t + l_t) - e_t$	$\lambda_{w,t}$ [\$/m^3/s]
$\underline{s}_{t+1} \leq s_{t+1} \leq \overline{s}_{t+1}$	*
$\underline{r}_t \leq r_t \leq \overline{r}_t$	*
$\widehat{P_t} \leq \varphi^h . \frac{s_{t+1}+s_t}{2} + \omega^h . r_t + \delta^h \quad \forall\ h = 1, \dots, H$	$\lambda^h_{HP,t}$ [\$/W]

*we considered that the maximum and minimum storage and release variables as a physical constraint that cannot be manipulated.

The lagrange multipliers $\lambda_{w,t}$ and $\lambda^h_{HP,t}$ (Table 7) indicate the added benefit if a marginal unit of inflow or power production could be increased. The optimal one-stage solution is found when its partial derivates with respect to each unknown variable is equated to zero, allowing to find the corresponding decision variables S_{t+1}, r_t and the constraints multipliers $\lambda_{w,t}$ *and* $\lambda^h_{HP,t}$ [Eq. (24) to Eq. (28)].

$$\frac{\partial Z}{\partial s_t} = \lambda_{w,t} + \sum_{h=1}^{H} \lambda^h_{HP,t} . \frac{\varphi^h}{2} = 0 \quad (24)$$

$$\frac{\partial Z}{\partial q_{t-1}} = \frac{\partial Z}{\partial q_t} . \frac{\partial q_t}{\partial q_{t-1}} = (\gamma_{t+1} + \lambda_{w,t}) . \left(\phi_t . \frac{\sigma_{q,t}}{\sigma_{q,t-1}}\right) = 0 \quad (25)$$

$$\frac{\partial Z}{\partial \lambda_{w,t}} = s_{t+1} - s_t - q_t + C^R(r_t + l_t) + e_t = 0 \quad (26)$$

$$\frac{\partial Z}{\partial \lambda^h_{HP,t}} = \widehat{P_t} - \varphi^h . \frac{s_{t+1} + s_t}{2} - \omega^h . r_t - \delta^h = 0 \quad (27)$$

$$\lambda^h_{HP,t} \geq 0 \quad (28)$$

Considering a finite planning horizon T and assuming that the benefit-to-go function at the last stage (F_{T+1}) is zero ($\alpha_{T+1} = \gamma_{T+1} = \beta_{T+1} = 0$), the parameters α_T, γ_T, and β_T can be calculated in the backward movement before transitioning to the next stage. These calculated parameters serve as input for the subsequent linear optimization. Consequently, the benefit function calculated in the current stage represents the future benefit function of the next stage in the backward movement [Eq. (29) to Eq. (31)].

$$Z = F_t(s_t, q_{t-1}) \leq \alpha_t . s_t + \gamma_t . q_{t-1} + \beta_t \quad (29)$$

$$\frac{\partial Z}{\partial s_t} = \alpha_t \quad (30)$$

$$\frac{\partial Z}{\partial q_{t-1}} = \gamma_t \quad (31)$$

Substituting [Eq. (24)] and [Eq. (25)] in [Eq. (30)] and [Eq. (31)], and knowing the lagrangean multipliers $\lambda_{w,t}$ *and* $\lambda^h_{HP,t}$ and the benefit-to-go function F_t, it is possible to find the new parameters $\alpha_t, \gamma_t, \beta_t$ [Eq. (32) to Eq.(34)].

$$\alpha_t = \lambda_{w,t} + \sum_{h=1}^{H} \lambda_{HP,t}^{h} . \frac{\varphi^h}{2} \tag{32}$$

$$\gamma_t = (\gamma_{t+1} + \lambda_{w,t}) . \left(\phi_t . \frac{\sigma_{q,t}}{\sigma_{q,t-1}} \right) \tag{33}$$

$$\beta_t = \mathrm{F_t}(\mathrm{s_t}, \mathrm{q_{t-1}}) - \alpha_t . s_t - \gamma_t . q_{t-1} \tag{34}$$

3.3.7.3 Inflow's stochasticity representation

To account for the stochasticity of reservoirs inflows q_t, the one-stage SDDP subproblem [Eq. (23)] is solved for K inflow branches/scenarios q_t^k (backward openings). Given a set of sampled hydrologic state variable q_{t-1}^o these K openings are estimated from the analytical built-in multi-site and multi-period autoregressive model of order p (MPAR(p)). The expected benefit-to-go function F_{t+1} is the expected value of the K benefit-to-go function F_{t+1}^k calculated for each inflow branch (Tilmant & Kelman, 2007).

Equation (35) represents the final benefit equation including k inflow scenarios, where the variables in bold represent vectors (of size J reservoirs) and the symbol $'$ represents the transpose vector. To calculate the vectors of parameters $\alpha_t^l, \gamma_t^l, \beta_t^l$ of the l^{th} cut that approximate the true benefit-to-go function F_{t+1}, at each stage, storages S_t^l are sampled for each l$^{\text{th}}$ cut and the corresponding $F_t^{l,k}$ probabilities for each inflow scenario must be summed. As the inflow scenarios were generated by a probabilistic model (MPAR), the average of the k results is assumed as final value [Eq. (36) to Eq.(38)].

$$Z = (HP_t - \boldsymbol{\zeta'}_t . \boldsymbol{z}_t) + (\boldsymbol{\alpha}_{t+1}^l . \boldsymbol{s'}_{t+1}^{l,k} + \boldsymbol{\gamma}_{t+1}^l . \boldsymbol{q'}_t^k + \boldsymbol{\beta}_{t+1}^l) + \tag{35}$$

$$\boldsymbol{\lambda}_{w,t}^{l,k} . (\boldsymbol{s}_{t+1} - \boldsymbol{s}_t^l - \boldsymbol{q}_t^k + \boldsymbol{C^R}(\boldsymbol{r}_t + \boldsymbol{l}_t) + \boldsymbol{e}_t) + \boldsymbol{\lambda}_{HP,t}^{l,h,k} . (\widehat{\boldsymbol{P_t}} - \boldsymbol{\varphi}^h . \frac{\boldsymbol{s'}_{t+1}^{l,k} + \boldsymbol{s'}_t^l}{2} - \boldsymbol{\omega}^h . \boldsymbol{r'}_t - \boldsymbol{\delta}^h)$$

$$\boldsymbol{\alpha}_t^l = \frac{1}{K} \sum_{k=1}^{K} \left(\boldsymbol{\lambda}_{w,t}^{l,k} + \sum_{h=1}^{H} \boldsymbol{\lambda}_{HP,t}^{l,h,k} . \frac{\boldsymbol{\varphi}^h}{2} \right) \tag{36}$$

$$\boldsymbol{\gamma}_t^l = \left(\gamma_{t+1}^l + \frac{1}{K} \sum_{k=1}^{K} (\boldsymbol{\lambda}_{w,t}^{l,k}) \right) . \left(\boldsymbol{\phi}_t . \frac{\boldsymbol{\sigma}_{q,t}}{\boldsymbol{\sigma}_{q,t-1}} \right) \tag{37}$$

$$\boldsymbol{\beta}_t^l = \frac{1}{K} \sum_{k=1}^{K} F_t^{l,k} - \boldsymbol{\alpha}_t^l . \boldsymbol{s}_t^l - \boldsymbol{\gamma}_t^l . \boldsymbol{q}_{t-1}^o \tag{38}$$

3.3.8 Preprocessing phase

Figure 20 and Figure 21 present the pseudocode used to generate the synthetics inflows for the backward and forward phases, respectively. The index t represents the stage of the time horizon and the index k represent the inflow scenario.

Sample q_{t-1}^{o} for $t = 1, \ldots, T$
For $t = 1, \ldots, T$
    For $k = 1, \ldots, K$
        Calculate $q_t^k = \mu_{q,t} + \phi_t . \frac{\sigma_{q,t}}{\sigma_{q,t-1}} . \left(q_{t-1}^0 - \mu_{q,t-1}\right) + \sigma_{q,t} . \epsilon_t$
    End
End

Figure 20. Preprocessing inflows' generation scenarios pseudo code for backward movement.

Sample q_0^m for $m = 1, \ldots, M$
Generate M synthetic inflow sequences q_t^m
For $t = 1, \ldots, T$
    For $m = 1, \ldots, M$
        Calculate $q_t^m = \mu_{q,t} + \phi_t . \frac{\sigma_{q,t}}{\sigma_{q,t-1}} . \left(q_{t-1}^m - \mu_{q,t-1}\right) + \sigma_{q,t} . \epsilon_t$
    End
End

Figure 21. preprocessing inflows' generation scenarios pseudo code for forward movement.

3.3.9 Backward phase

During the backward optimization, an upper bound to the true benefit-to-go function F_{T+1} is calculated at the sampled points. We assume that the benefit-to-go F_{T+1} at the last stage T is nonexistent (zero) [Eq. (39)].

$$\alpha_{T+1}^{l} = \gamma_{T+1}^{l} = \beta_{T+1}^{l} = 0 \tag{39}$$

Figure 22 presents the pseudo code used in the backward optimization phase. At each stage t, $\boldsymbol{s}_t^l$ and $\boldsymbol{q}_{t-1}^o$ are sampled and $F_t^{l,k}$ is calculated. The resulting benefit-to-go functions at the initial stage $F_1^l(\boldsymbol{s}_1^l, q_0^o)$ represents the immediate benefits plus the expected benefits from the beginning to the end of the planning period (1 to T) for each storage sampled $\boldsymbol{s}_1^l$. It is therefore an upper bound to the "true" function (40). The accuracy of this approximation is evaluated by the forward simulation phase.

$$Z \leq \overline{Z} \tag{40}$$

J = number of reservoirs of the hydro-system
K = number of inflow scenarios
L = number of cuts that approximate the benefit to go function
T = length of the planning horizon

Initialize $\alpha_{T+1}^{l} = 0;\ \gamma_{T+1}^{l} = 0;\ \beta_{T+1}^{l} = 0$ for $l = 1,\ \ldots,\ L$
For $t\ =\ T,\ T-1,\ \ldots,1$
    For $l = 1,\ \ldots, L$
        Sample s_t^l
        Retrieve $\alpha_{t+1}^{l};\ \gamma_{t+1}^{l};\ \beta_{t+1}^{l}$
        For $k = 1,\ \ldots, K$
            Retrieve synthetic inflow q_t^k
            Calculate one-stage problem $\lambda_{w,t}^{l,k};\ \lambda_{HP,t}^{l,h,k}; S_{t+1}^{l,k}; F_t^{l,k}$
        End
        Calculate $\alpha_t^l,\ \gamma_t^l,\ \beta_t^l$
    End
End
Calculate the upper bound $\bar{Z}$

Figure 22. Backward optimization phase pseudo-code (adapted from Quentin Goor (2010)).

3.3.10 Forward phase

Simulating the system forward gives a lower bound $\underline{Z}$ to the solution of the multistage decision-making problem. Selecting an initial storage $\boldsymbol{s}_1$ (e.g., $\boldsymbol{s}_1^1$ of the backward phase), the forward simulation procedure applies the mass balance equation (8) to find the storage $\boldsymbol{s}_{t+1}$, and the cuts generated in the backwards procedure [Eq. (36) to (38)] to calculate the F_t at each stage. The sum of the immediate benefits found at each stage gives the optimal result, and considering a tolerance θ, it is equivalent to the $F_1^1(\boldsymbol{s}_1^1, q_0^o)$ value found in the backward phase [Eq. (41)].

$$\overline{Z} = \underline{Z} + \theta \tag{41}$$

The forward phase sets several hydrologic sequences in order to estimate the expected benefit as the mean benefit over all simulation scenarios [Eq. (43) to (45)].

$$F_t^m = f_t^m(s_t, q_t^m, r_t) + \boldsymbol{\alpha}_{t+1}^{l}.\boldsymbol{s'}_{t+1} + \boldsymbol{\gamma}_{t+1}^{l}.\boldsymbol{q'}_t^m + \boldsymbol{\beta}_{t+1}^{l} \tag{42}$$

$$Z^m = \sum_{t=1}^{T} f_t^m(s_t, q_t^m, r_t) \tag{43}$$

The mean benefit over all simulation scenarios is given by [Eq. (44)] and the standard deviation of the estimated lower bound can also be calculated by [Eq. (45)].

$$\underline{Z}_{\mu} = \frac{Z^m}{M} \tag{44}$$

$$\underline{Z}_{\sigma} = \sqrt{\frac{1}{M-1}\sum_{m=1}^{M}(Z^m - \underline{Z}_{\mu})^2} \tag{45}$$

The tolerance θ is given by 95% confidence interval around the estimated value of $\underline{Z}$.

$$\theta \in \left[\underline{Z}_{\mu} - 1.96\frac{\underline{Z}_{\sigma}}{\sqrt{M}}, \underline{Z}_{\mu} + 1.96\frac{\underline{Z}_{\sigma}}{\sqrt{M}}\right] \quad (46)$$

Figure 23 presents the pseudo code used in the forward simulation phase.

M = number of inflow scenarios
L = number of cuts that approximate the benefit to go function
T = length of the planning horizon
Select an initial storage s_1

For $m = 1, \ldots, M$
    For $t = 1, \ldots, T$
        Retrieve α_t^l, γ_t^l, β_t^l for all $l = 1, \ldots, \mathrm{L}$ (from backward move)
        Retrieve synthetic inflow q_t^m
        For $l = 1, \ldots, L$
            Solve the one stage problem F_t^m
            Save $f_t^m(s_t, q_t^m, r_t)$
        End
    End
    Calculate Z^m
End
Calculate the lower bound $\underline{Z}$

Figure 23. Forward simulation phase pseudo-code (adapted from Quentin Goor (2010)).

3.3.11 Convergence check

If $\overline{Z}$ is within the confidence interval [Eq. (46)], then the approximation is statistically acceptable. Otherwise, a new iteration is executed with an additional set of storage samples. This backward phase is then followed by a new forward simulation, which will exploit the cuts that have been generated during the previous backward recursions. The process is repeated until convergence.

3.4 Application

3.4.1 The Paraná River Basin hydropower system

The study area includes the upper Paraná River Basin, which encompasses a total of 65 hydropower plants connected to the National Integrated System (SIN). Specifically, 56 of these hydropower plants are situated upstream of the Itaipu dam, as depicted in Figure 24. For the purpose of this study, the system operation boundary was defined to encompass the hydropower plants and their respective reservoirs located upstream and including the Itaipu hydropower plant. This boundary delineation allows for directly influence on the target environmental site.

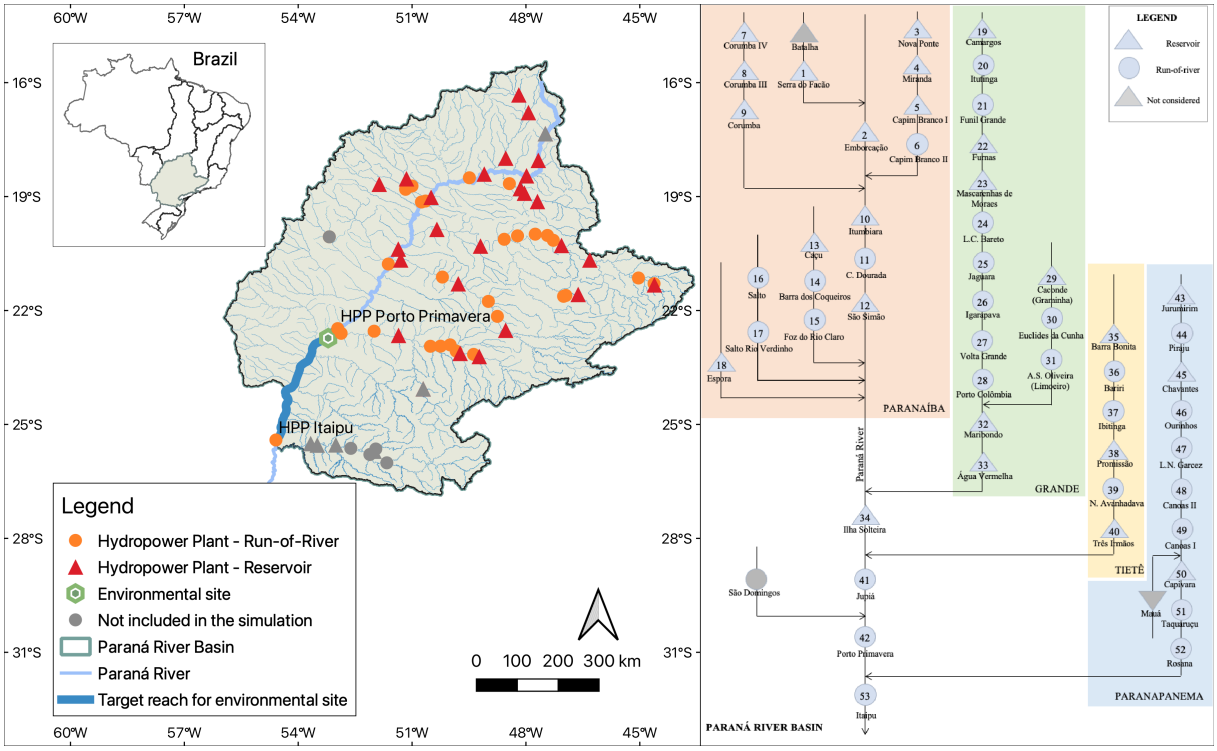

Figure 24. Hydropower plant's location in the Upper Paraná River Basin.

3.4.2 Modeling representation

In Brazil, the concept of firm energy refers to the maximum continuous energy production achievable by a hydropower plant, considering the occurrence of the driest sequence ever recorded in the river's flow history at the plant's location (Aneel, 2005). This firm energy value is further adjusted to account for a long-term non-attendance risk of 5% and serves as the basis for establishing power purchase agreements (Barros et al., 2003). Any energy generated above the firm energy level is referred to as secondary energy.

The model takes into account the hydropower generation of individual hydropower plants, considering both firm power and secondary power categories [Eq. (47)]. The optimization of generation is performed throughout the planning period with the following considerations: (a) Prioritizing the fulfillment of firm power generation, which is associated with higher benefits and (b) Generating secondary energy when feasible.

$$\hat{P}_t = \hat{P}_{firm,t} + \hat{P}_{sec,t} \tag{47}$$

In a current and future wet scenario, where the generation of secondary energy does not impact future firm power generation, both energy types can be generated concurrently throughout the planning period. This allows for the utilization of available water resources to generate both firm and secondary energy.

In a current dry and future wet scenario, the model can choose to generate both firm and secondary energy in the present (if feasible) to avoid potential spillage losses in the future. However, if it is not possible to generate both energies, the model prioritizes the generation of firm energy to meet the demand.

In a current wet and future dry scenario, the model focuses on generating only the firm energy and storing the surplus water to ensure the availability of firm energy generation in the future when water resources are expected to be scarce.

In dry current and future scenarios, both firm and secondary energy generation can be affected. In such situations, the deficit in energy generation may need to be supplemented by thermopower generation or hydropower transfer from regions with higher storage levels. It is important to note that this study does not include the modeling of thermopower complementation or hydropower transfer between different basins.

3.4.3 Input variables

Table 8 summarizes the input variables and the corresponding references used to configurate the SDDP model.

Table 8. SDDP optimization model Input data.

Input data	Data Type	Variable	Equation	Reference
Reservoir natural inflows(1) [m^3/s]	Monthly time-series (1994 – 2019)	q_t, q_{t-1}	(9)	(ANA), 2020)
Net reservoir evaporation [mm/month]	Monthly average time series	e_t	(8)	(CCEE, 2020)
Reservoir head [m]	Level x Area x Volume Curves	h	(10)	(CCEE, 2020)
Reservoir max and minimum storage [hm^3]	Level x Area x Volume Curves	$\overline{S}_t$ *and* $\underline{S}_t$	(3)	(CCEE, 2020)
Reservoir initial storage [hm^3]	Historical daily time series	S_t^o	(35)	(ANA), 2020)
Maximum and minimum turbined outflow [m^3/s]	Hydropower plant Technical data	$\overline{r}_t$ and $\underline{r}_t$	(4)	(ANA), 2020) (CCEE, 2020)
Hydropower plants' capacity [MW]	Hydropower plant Technical data	P_{max}	(12)	(ONS, 2020)
Hydropower plants' firm energy [MW]	Hydropower plant Operational data	$\hat{P}_{firm,t}$	(47)	(Aneel, 2005) (MME, 2017)
Energy price(2) [R$/MWh]	Average price of hydraulic energy	π_t	(13)	(MME, 2020)
Operation and maintenance costs	Not used	θ	(13)	-
Penalty costs	Calibration variable	ζ_t	(14)	-
Turbine efficiency(3)	Technical data and operational time series	η	(10)	(ANA), 2020) (CCEE, 2020)
Number of inflow scenarios (simulation phase)	20	M	(42)	-
Number of inflow scenarios (backward phase)	30	K	(35)-(38)	-
Time step	month	t	-	-

(1) The natural incremental (lateral) inflows of each reservoir of the Parana hydro-system were calculated based on the natural inflows, which disregard the operational effects of the upstream reservoirs' cascade and the reservoir evaporation. The historical daily time series were converted to monthly average time series.

(2) It was used a fixed energy price for all hydropower plants and months based on the average price of hydraulic energy.

(3) The turbine efficiency of each hydropower plant was calculated as the monthly average of the quotient between the observed energy generated and the theoretical energy that would be generated by the same observed inputs with 100% of efficiency (see equation (10)). It was used a fixed turbine efficiency for each hydropower plant (i.e., head effect on the efficiency were not considered).

Table 9 provides an overview of the key technical and operational characteristics of the hydropower plants included in the simulation. The highlighted hydropower plants in the table represent the ten facilities with the highest installed capacity. These ten plants collectively account for 73% of the total installed capacity and 67% of the total reservoir storage capacity within the system.

Table 9. Technical data of modeling hydropower plants. Source: CCEE (2020).

Id	Name	Min Storage [hm^3]	Max Storage [hm^3]	Max Release [m^3/s]	Capacity [MW]
1	Serra do facão	1,752.0	5,199.0	324.0	212.6
2	Emborcação	4,669.0	17,725.0	1,048.0	1,192.0
3	Nova Ponte	2,412.0	12,792.0	576.0	510.0
4	Miranda	974.0	1,120.0	675.0	408.0
5	Capim Branco I (Amador Aguiar I)	228.3	241.1	495.0	240.0
6	Capim Branco II (Amador Aguiar II)	878.0	879.0	537.0	210.0
7	Corumbá IV	2,936.6	3,708.0	208.0	127.0
8	Corumbá III	709.0	972.0	278.0	96.4
9	Corumbá I	470.0	1,500.0	570.0	375.0
10	Itumbiara	4,573.0	17,027.0	2,940.0	2,082.0
11	Cachoeira Dourada	460.0	460.0	2,513.0	658.0
12	São Simão	7,000.0	12,540.0	2,670.0	1,710.0
13	Caçu	195.8	227.5	268.0	65.0
14	Barra dos coqueiros	300.0	347.8	278.0	90.0
15	Foz do Rio Claro (Eng. J.L.M Godoy)	95.3	95.3	298.0	68.4
16	Salto	826.1	826.1	260.0	116.0
17	Salto do Rio Verdinho	264.5	264.5	254.0	93.0
18	Espora	71.0	209.0	72.0	32.1
19	Camargos	120.0	792.0	220.0	46.0
20	Itutinga	11.0	11.0	236.0	52.0
21	Funil	304.0	304.0	585.0	180.0
22	Furnas	5,733.0	22,950.0	1,692.0	1,312.0
23	Mascarenhas de Moraes (Peixoto)	1,540.0	4,040.0	1,328.0	478.0
24	Luiz Carlos Barreto (Estreito)	1,423.0	1,423.0	2,028.0	1,104.0
25	Jaguara	450.0	450.0	1,076.0	424.0
26	Igarapava	480.0	480.0	1,480.0	210.0
27	Volta Grande	2,244.0	2,244.0	1,584.0	380.0
28	Porto Colômbia	1,524.0	1,524.0	1,988.0	328.0
29	Caconde	51.0	555.0	94.0	80.4
30	Euclides da cunha	14.0	14.0	148.0	108.8
31	Armando Salles de Oliveira (Limoeiro)	25.0	25.0	178.0	32.0
32	Marimbondo	890.0	6,150.0	2,944.0	1,488.0

33	Água vermelha (J. Ermirio de Moraes)	5,856.0	11,025.0	2,958.0	1,396.2
34	Ilha Solteira	8,232.0	21,060.0	9,399.0	3,444.0
35	Barra Bonita	569.0	3,135.0	756.0	140.0
36	Bariri (Álvaro de Souza Lima)	544.0	544.0	771.0	144.0
37	Ibitinga	985.0	985.0	702.0	131.4
38	Promissão (Mário Lopes Leão)	5,280.0	7,408.0	1,293.0	264.0
39	Nova Avanhandava (Rui Barbosa)	2,720.0	2,720.0	1,431.0	347.4
40	Três Irmãos	9,923.0	13,372.0	2,180.0	807.5
41	Jupiá (Eng. Souza Dias)	3,354.0	3,354.0	8,344.0	1,551.2
42	Porto Primavera (Eng. Sérgio Motta)	14,400.0	14,400.0	8,904.0	1,540.0
43	Jurumirim (A. Avellanal Layder)	3,843.0	7,008.0	364.0	101.0
44	Piraju	84.0	84.0	362.0	80.0
45	Chavantes	5,754.0	8,795.0	626.0	414.0
46	Ourinhos	20.8	20.8	486.0	44.1
47	L.N. Garcez (Salto Grande)	45.0	45.0	580.0	74.0
48	Canoas II	151.0	151.0	561.0	72.0
49	Canoas I	212.0	212.0	567.0	82.5
50	Capivara (E. Engenharia Mackenzie)	4,816.0	10,540.0	1,520.0	643.0
51	Taquaruçu (Escola Politécnica)	677.0	677.0	2,550.0	525.0
52	Rosana	1,918.0	1,918.0	2,468.0	354.0
53	Itaipu	23,337.5	29,403.9	13,260.0	14,000.0

3.4.4 Optimization procedure: finding the benefit-to-go functions

To determine the benefits-to-go functions, the SDDP model was executed in monthly time steps over a 10-year period (T = 120 stages), utilizing k=30 backward openings and M=20 simulation sequences. A ten-year period was chosen since it provides enough room to avoid the influence of initial conditions and allows the system to find a near steady-state operating function, as detailed in 3.3.6. Backward openings and simulation sequences were chosen based on pre-processing analysis, which aimed to find improved computational performance without interfering with the results performance.

It is important to note that the cuts assumed at the final stage (T+1) can significantly impact the reservoirs' release decisions. For example, if zero future benefits are assumed for the final stage, the model might prioritize utilizing all storage volume in previous stages to generate electricity and maximize benefits instead of reserving a surplus for future needs (Rougé & Tilmant, 2016). To address this issue, we conducted the model in two consecutive runs. In the second run, we applied the cuts obtained from the first run at the final period.

3.4.5 Reoptimization procedure: simulating the hydropower system operation

For SDP models, Tejada-Guibert et al. (1993) proposed finding a steady-state operating condition of the system through iterative runs. This condition is then utilized to simulate optimal operating policies (releases) over longer periods. In the context of SDDP modeling, Rougé & Tilmant (2016) introduced the year-periodic reoptimization (YPRE) procedure. This procedure utilizes year-specific cuts (benefit-to-go functions) obtained from a near steady-state condition during the optimization process and applies these cuts to each year of the simulation horizon to find the optimal operating policies (releases).

In our study, we selected the cuts from the fourth year of the 10-year optimization period (artificially extended by considering the cuts of the first run at the final period of the second run) as the near steady-state condition. We chose this year after verifying that it was not biased by neither the initial conditions or end of period (Figure 25).

Finally, the simulation was then run for a planning horizon T=108 months, from 2011 to 2019 using the historical hydrological data. This period encompasses the full construction and operation of the modeled hydropower plants in the basin. The initial reservoirs' storage was set according to the reservoirs' storage in the first day of 2011 and the natural hydropower plants inflows spanning from 2011 to 2019. The results were compared with the historical operation for the same period.

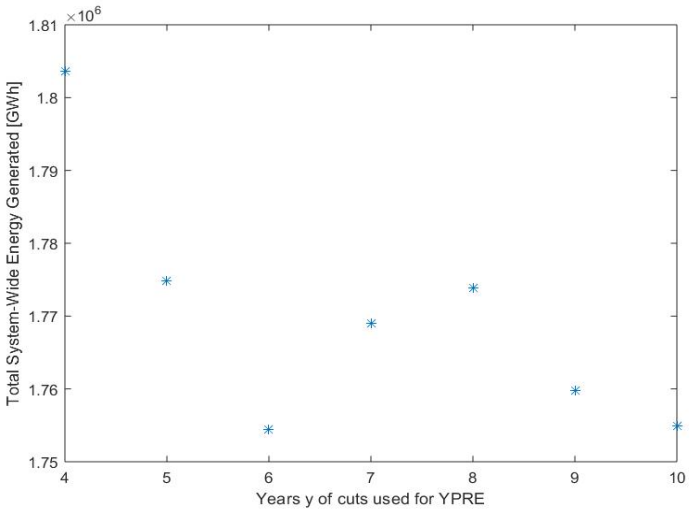

Figure 25. System-wide benefits over the 8 simulation years using the YPRE procedure.

3.5 Results

3.5.1 Convergence: forward and backward movement

The model runs converged after 15 iterations (Figure 26).

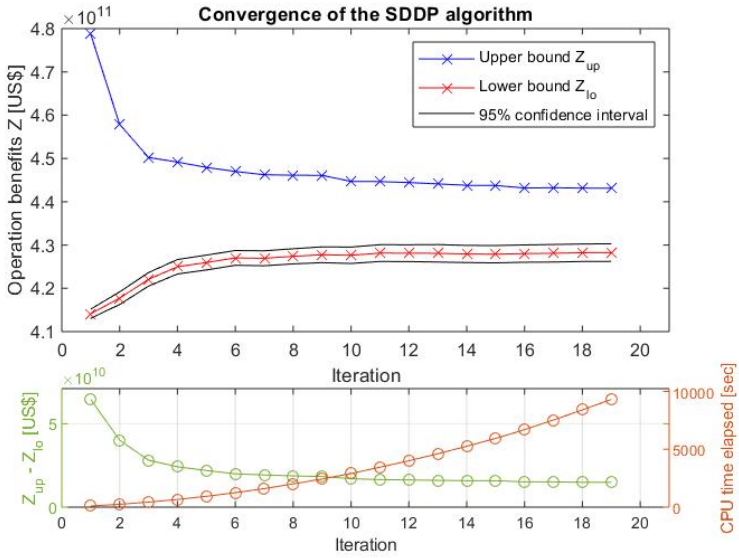

Figure 26. Convergence of the SDDP run.

3.5.2 Observed energy versus Simulated energy

Table 10 compares the total observed energy and the total simulated energy produced by each hydropower plant during the simulated period (2011-2019). The mean error (2.85%) indicates the consistency of the model in reproducing the operation, despite the modeled region including a part of the whole SIN. A higher value was anticipated since real operating decisions involve additional factors not considered in this study (e.g., shutdowns for maintenance or political decisions), which can reduce or alter the generation distribution.

Table 10. Individual observed energy versus simulated energy produced from 2011 to 2019.

Id	Name	Total energy produced [GWh] - Observed (2011 - 2019)	Total energy produced [GWh] - Simulated (2011 - 2019)	Error (%)
1	Serra do facão	5,572.3	6,195.6	11.18
2	Emborcação	25,170.0	26,053.8	3.51
3	Nova Ponte	15,017.6	16,153.1	7.56
4	Miranda	12,711.7	10,057.9	-20.88
5	Capim Branco I (Amador Aguiar I)	10,530.3	8,112.8	-22.96
6	Capim Branco II (Amador Aguiar II)	9,095.8	6,592.8	-27.52
7	Corumbá IV	3,742.8	4,056.9	8.39
8	Corumbá III	2,578.9	2,833.2	9.86
9	Corumbá I	14,086.3	15,124.1	7.37
10	Itumbiara	50,532.9	52,265.4	3.43
11	Cachoeira Dourada	23,474.8	22,139.4	-5.69
12	São Simão	88,638.5	89,937.8	1.47
13	Caçu	3,043.6	3,059.6	0.52
14	Barra dos coqueiros	4,212.3	4,414.4	4.80
15	Foz do Rio Claro (Eng. J.L.M Godoy)	3,329.7	3,301.2	-0.85
16	Salto	5,616.6	5,496.0	-2.15
17	Salto do Rio Verdinho	4,886.7	4,839.2	-0.97
18	Espora	2,125.8	2,050.7	-3.54
19	Camargos	1,124.2	1,437.3	27.85
20	Itutinga	1,583.3	1,571.2	-0.76
21	Funil	7,041.3	4,336.9	-38.41
22	Furnas	32,854.9	31,209.5	-5.01
23	Mascarenhas de Moraes (Peixoto)	17,262.2	17,288.0	0.15
24	Luiz Carlos Barreto (Estreito)	28,095.0	30,105.0	7.15
25	Jaguara	19,404.1	20,862.9	7.52
26	Igarapava	8,388.3	8,024.1	-4.34
27	Volta Grande	14,219.3	14,444.5	1.58
28	Porto Colômbia	13,731.3	11,441.8	-16.67
29	Caconde	2,286.5	2,730.3	19.41
30	Euclides da cunha	3,304.5	3,770.6	14.10
31	Armando Salles de Oliveira (Limoeiro)	959.9	948.2	-1.22
32	Marimbondo	46,511.4	50,013.0	7.53
33	Água vermelha (José Ermirio de Moraes)	53,380.9	58,512.1	9.61
34	Ilha Solteira	123,693.8	127,758.8	3.29

35	Barra Bonita	4,854.9	5,792.2	19.31
36	Bariri (Álvaro de Souza Lima)	5,817.2	6,473.3	11.28
37	Ibitinga	6,096.9	7,500.3	23.02
38	Promissão (Mário Lopes Leão)	9,929.0	11,267.0	13.48
39	Nova Avanhandava (Rui Barbosa)	12,605.1	13,480.7	6.95
40	Três Irmãos	21,052.2	23,866.3	13.37
41	Jupiá (Eng. Souza Dias)	71,464.3	77,756.3	8.80
42	Porto Primavera (Eng. Sérgio Motta)	83,263.5	85,172.0	2.29
43	Jurumirim (A. Avellanal Layder)	4,960.6	5,069.4	2.19
44	Piraju	3,876.1	3,809.1	-1.73
45	Chavantes	16,822.4	16,874.2	0.31
46	Ourinhos	1,937.3	2,309.1	19.19
47	L.N. Garcez (Salto Grande)	4,378.7	4,340.2	-0.88
48	Canoas II	4,282.4	4,390.1	2.52
49	Canoas I	5,006.4	5,148.8	2.84
50	Capivara (E. Engenharia Mackenzie)	31,887.4	36,930.4	15.82
51	Taquaruçu (Escola Politécnica)	21,401.0	21,395.8	-0.02
52	Rosana	19,337.5	16,157.6	-16.44
53	Itaipu	734,548.6	755,931.9	2.91
TOTAL		**1,721,729.2**	**1,770,803.2**	**2.85**

3.5.3 Annual and monthly energy production behavior

Figure 27 illustrates the comparison between the annual observed energy and the annual simulated energy from 2011 to 2019 in the cascade hydropower system of the study area, along with the monthly energy production variability. Following that, Figure 28 presents the annual energy production of the ten hydropower plants with the highest installed capacity.

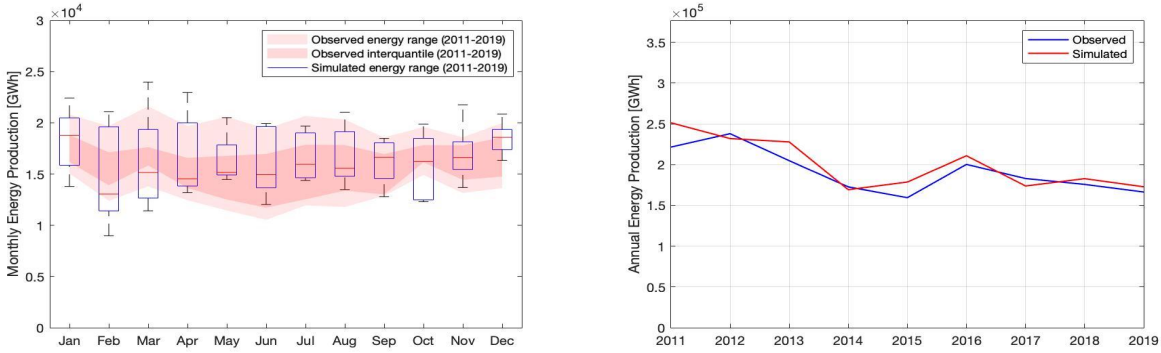

Figure 27. Comparison between simulated x observed monthly energy produced.

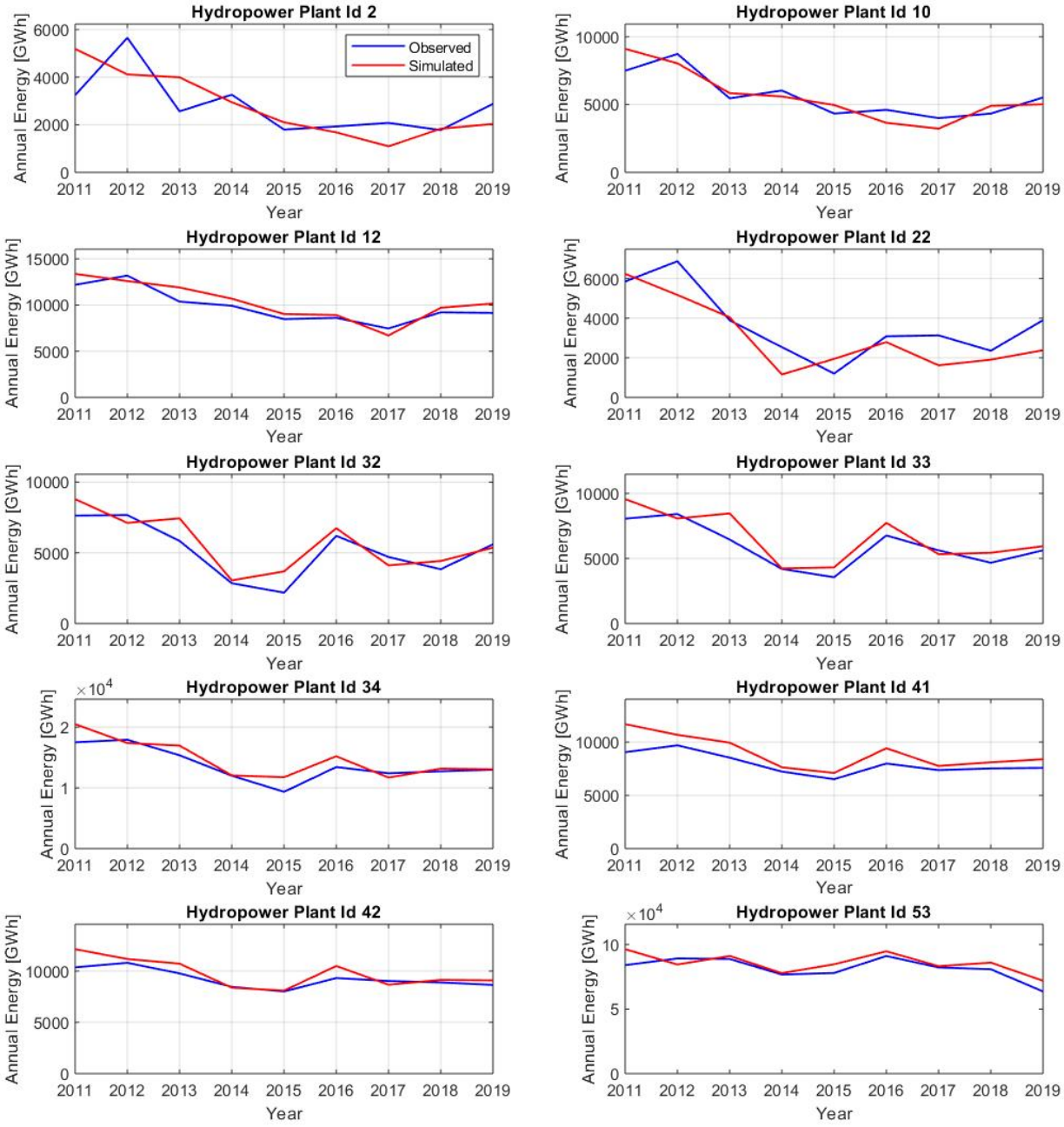

Figure 28. Comparison between simulated x observed annual energy produced.

Table 11 shows the performance results based on two evaluation metrics: the Nash-Sutcliffe coefficient (NS) and the coefficient of determination (r^2) (Krause et al., 2005). Most hydropower plants presented coefficients (r^2 and NS) above 0.9, which indicates the consistency of the model to represent the individual hydropower plants' operation.

Table 11. Performance coefficients of Annual Energy Production.

Id	Hydropower Plant	r^2 (1)	NS (2)
2	Emborcação	0.396	0.151
10	Itumbiara	0.941	0.935
12	São Simão	0.992	0.985
22	Furnas	0.681	0.669
32	Marimbondo	0.934	0.907

33	Água vermelha (José Ermirio de Moraes)	0.966	0.921
34	Ilha Solteira	0.989	0.981
41	Jupiá (Eng. Souza Dias)	0.992	0.945
42	Porto Primavera (Eng. Sérgio Motta)	0.993	0.984
53	Itaipu	0.997	0.994

(1) $r^2 = \left(\frac{\sum_{i=1}^{I}(O_i-\bar{O})(P_i-\bar{P})}{\sqrt{\sum_{i=1}^{I}(O_i-\bar{O})^2}\sqrt{\sum_{i=1}^{I}(P_i-\bar{P})^2}} \right)^2$ (2) $NS = 1 - \frac{\sum_{i=1}^{I}(O_i-P_i)^2}{\sum_{i=1}^{I}(O_i-\bar{O})^2}$

where i represents the register number, O_i is the observed output at i; P_i is the predicted output at i; $\bar{O}$ is the mean of the observed output; $\bar{P}$ is the mean of the predicted output; I is the total number of samples.

3.6 Conclusion

In this chapter we investigated the applicability of a hydro-economic model based on the Stochastic Dual Dynamic Programming (SDDP) method to simulate the energy production of the individual hydropower plants of the Paraná River Basin, which is part of the Brazilian country large-scale power system. We conclude that the model replicated and captured the primary patterns of historical reservoir operation, yielding accurate results for a significant portion of the observed operational range even though only a part of the whole Brazilian power system (SIN) is modeled. The model overall overestimated the energy production (by 2.85% in total), which suggests that intervening factors driving the operation of the whole integrated system may produce decisions that cannot be totally explained by the input variables applied in this study.

Despite the limitations, the model shows potential to be applied under different hydroclimatic scenarios and water user demands to enhance our understanding of water use trade-offs. The improved understanding and identification of trade-offs can contribute to the development of more effective strategies for managing future water use. This is particularly crucial in the study area where the operation of reservoirs has posed challenges to the natural equilibrium of the river basin, thereby rendering ecosystems and communities vulnerable.

3.7 Appendix I. MPAR autoregressive model

A Periodic Autoregressive (PAR) model is a type of time series model that incorporates both autoregressive components and periodic patterns. It's specifically designed to capture periodic fluctuations or seasonality in time series data. In a PAR(p) model, the autoregressive part captures the dependencies of the current value on its past values, similar to traditional AR models. The term "order" refers to the number of lagged values of the variable being predicted that are used as predictors in the model. For order p equal to one, the model uses only the most recent lagged value (t-1) of the variable to predict its current value.

In addition to this autoregressive component, a multi periodic MPAR model includes terms that account for the periodic patterns inherent in the data. By including both autoregressive and periodic terms, PAR models can effectively capture both short-term dependencies and longer-term periodic patterns in the data.

Equation (48) shows the general form a MPAR model of order 1.

$$\left(\frac{q_t(j)-\mu_{q,t}(j)}{\sigma_{q,t}(j)}\right)=\phi_t(j).\left(\frac{q_{t-1}(j)-\mu_{q,t-1}(j)}{\sigma_{q,t-1}(j)}\right)+\epsilon_t(j) \quad (48)$$

where:

The indexes j and t represent the reservoir and time-step; ϕ_t is the autoregressive coefficient of order 1; $\mu_{q,t}(j)$ and $\sigma_{q,t}(j)$ represent the periodic mean and standard deviation for each time-step. For example, for monthly time-steps, they represent the mean and standard deviation of the given month of the year; $\epsilon_t(j)$ represents the stochastic noise.

A stochastic noise of zero mean and with constant variance describes random variations in data that, on average, do not introduce any systematic bias (since the mean is zero), but they do exhibit a level of variability or dispersion around that mean. The constant noise indicates that the model is not making larger errors in predicting prices for higher flow values compared to lower-flow ones.

Implementing this model requires estimating the autoregressive coefficient ϕ_t and the mean and standard deviation parameters for each time-step. It is possible to use techniques like least squares estimation, maximum likelihood estimation, or other suitable optimization methods to fit the model to data.

3.8 Appendix II. Code and Programs Information

The code adaptations in this study were designed by the author using the MATLAB (version R2021a) language.

3.9 References

Agência Nacional de Águas (ANA). (2020). SAR - Sistema de acompanhamento de reservatórios. Retrieved from https://www.ana.gov.br/sar/

Aneel. (2005). Cadernos temáticos Aneel - Energia assegurada. Brasília, DF.

Barros, M. T. L., Tsai, F. T.-C., Yang, S., Lopes, J. E. G., & Yeh, W. W.-G. (2003). Optimization of Large-Scale Hydropower System Operations. Journal of Water Resources Planning and Management, 129(3), 178–188. https://doi.org/10.1061/(ASCE)0733-9496(2003)129:3(178)

Boschetti, M., & Maniezzo, V. (2009). Benders decomposition, Lagrangean relaxation and metaheuristic design. Journal of Heuristics, 15(3), 283–312. https://doi.org/10.1007/s10732-007-9064-9

CCEE. (2020). Hydroedit - apoio à leitura de arquivos. Retrieved December 10, 2020, from https://www.ccee.org.br/acervo-ccee?especie=44884&keyword=hydroedit&periodo=5000

Cicogna, M. A. (2003). Sistema de suporte a decisão para o planejamento e a programação da operação de sistemas de energia eletrica. Universidade Estadual de Campinas. Retrieved from http://repositorio.unicamp.br/bitstream/REPOSIP/260310/1/Cicogna_MarceloAugusto_D.pdf

Cicogna, M. A., & Filho, S. S. (2006). Hydrolab. São Paulo. Retrieved from https://docs.google.com/viewer?a=v&pid=sites&srcid=ZGVmYXVsdGRvbWFpbnxzaXN0ZW1hc2hpZHJvdGVybWljb3N8Z3g6NjlkZTMwMjliN2I5OTgxNg

Eletrobras. (2020). Newave and Decomp models - reservoir operating policies. Retrieved from http://www.cepel.br/pt_br/produtos/decomp-modelo-de-planejamento-da-operacao-de-sistemas-hidrotermicos-interligados-de-curto-prazo.htm

EPE. (2022). Brazilian Energy Balance 2022. Brasília, DF. Retrieved from https://www.epe.gov.br/sites-pt/publicacoes-dados-abertos/publicacoes/PublicacoesArquivos/publicacao-675/topico-638/BEN2022.pdf

Giuliani, M., Lamontagne, J. R., Reed, P. M., & Castelletti, A. (2021). A State-of-the-Art Review of Optimal Reservoir Control for Managing Conflicting Demands in a Changing World. Water Resources Research, 57(12). https://doi.org/10.1029/2021WR029927

Gjelsvik, A., Mo, B., & Haugstad, A. (2010). Long- and Medium-term Operations Planning and Stochastic Modelling in Hydro-dominated Power Systems Based on Stochastic Dual Dynamic Programming (pp. 33–55). https://doi.org/10.1007/978-3-642-02493-1_2

Goor, Q., Kelman, R., & Tilmant, A. (2011). Optimal Multipurpose-Multireservoir Operation Model with Variable Productivity of Hydropower Plants. Journal of Water Resources Planning and Management, 137(3), 258–267. https://doi.org/10.1061/(ASCE)WR.1943-5452.0000117

Goor, Quentin. (2010). Optimal operation of multiple reservoirs in hydropower-irrigation systems : a stochastic dual dynamic programming approach, 150. Retrieved from http://hdl.handle.net/2078.1/69103

Hidalgo, I. G., Paredes-Arquiola, J., Andreu, J., Lerma-Elvira, N., Lopes, J. E. G., & Cioffi, F. (2020). Hydropower generation in future climate scenarios. Energy for Sustainable Development, 59, 180–188. https://doi.org/10.1016/j.esd.2020.10.007

Krause, P., Boyle, D. P., & Bäse, F. (2005). Comparison of different efficiency criteria for hydrological model assessment. Advances in Geosciences, 5, 89–97. https://doi.org/10.5194/adgeo-5-89-2005

MME. Portaria 178 de 3 de maio de 2017 (2017). Brasil. Retrieved from https://www.epe.gov.br/sites-pt/publicacoes-dados-abertos/publicacoes/PublicacoesArquivos/publicacao-352/topico-463/prt2017178mme.pdf

MME. RESOLUÇÃO NORMATIVA No 908, DE 15 DE DEZEMBRO DE 2020 (2020). Brasil. Retrieved from https://www.in.gov.br/en/web/dou/-/resolucao-normativa-n-908-de-15-de-dezembro-de-2020-295257873

ONS. (2020). Brazil hydro-thermal-wind system. Retrieved from http://www.ons.org.br/paginas/sobre-o-sin/o-que-e-o-sin

ONS. (2023). Plano de Operação Energético 2019-2023. Brasília, DF. Retrieved from https://www.ons.org.br/AcervoDigitalDocumentosEPublicacoes/PEN_Executivo_2019-2023.pdf

Pereira, M. V. F., & Pinto, L. M. V. G. (1985). Stochastic Optimization of a Multireservoir Hydroelectric System: A Decomposition Approach. Water Resources Research, 21(6), 779–792. https://doi.org/10.1029/WR021i006p00779

Rougé, C., & Tilmant, A. (2016). Using stochastic dual dynamic programming in problems with multiple near-optimal solutions. Water Resources Research, 52(5), 4151–4163.

https://doi.org/10.1002/2016WR018608

Santos, E. P. (2015). Modelo de programação da operação de sistemas hidrelétricos com restrição de segurança. Tese de doutorado: UNICAMP.

Tejada-Guibert, J. A., Johnson, S. A., & Stedinger, J. R. (1993). Comparison of two approaches for implementing multireservoir operating policies derived using stochastic dynamic programming. Water Resources Research, 29(12), 3969–3980. https://doi.org/10.1029/93WR02277

Tilmant, A., & Kelman, R. (2007). A stochastic approach to analyze trade-offs and risks associated with large-scale water resources systems. Water Resources Research, 43(6). https://doi.org/10.1029/2006WR005094

Tilmant, A., Pinte, D., & Goor, Q. (2008). Assessing marginal water values in multipurpose multireservoir systems via stochastic programming. Water Resources Research, 44(12). https://doi.org/10.1029/2008WR007024

Van de Water, H., & Willems, J. (1981). The certainty equivalence property in stochastic control theory. IEEE Transactions on Automatic Control, 26(5), 1080–1087. https://doi.org/10.1109/TAC.1981.1102781

Zambon, R. C., Barros, M. T. L., Lopes, J. E. G., Barbosa, P. S. F., Francato, A. L., & Yeh, W. W.-G. (2012). Optimization of Large-Scale Hydrothermal System Operation. Journal of Water Resources Planning and Management, 138(2), 135–143. https://doi.org/10.1061/(ASCE)WR.1943-5452.0000149

CHAPTER 4

The Role of Reservoir Reoperation to Mitigate Climate Change Impacts on Hydropower and Environmental Water Demands

This chapter has been published and it can be found under https://doi.org/10.1061/JWRMD5.WRENG-5810.

CHAPTER 5

Dynamic Adaptive Environmental Flows (DAE-flows) to Reconcile Long-term Ecosystem Demands with Hydropower Objectives

This chapter has been published and it can be found under https://doi.org/10.1029/2022WR034064.

CHAPTER 6

The Electricity Market as Institutional and Financial Arrangement to Restore Environmental Flow Regimes in Hydropower Basins

CHAPTER 7

The Economic Value of Hydrometeorological Information in the Planning of Large-scale Hydropower Systems Operation

CHAPTER 8

Final Conclusion and Policy Implications

The development of this work has allowed several insights that lead to some key policy implications, as well as technical and specific learnings.

The findings indicate that we can enhance the capacity of water systems to incorporate historically suppressed environmental water demands without imposing a hard constraint to economic uses. Defining the ecosystem functions to be restored and developing ecological-flow relationships enables the quantification of environmental performance and trade-offs.

Improving reservoir operating strategies is particularly crucial when facing drier conditions. Reoperation can work as an adaptive measure not only to mitigate energy losses under a changing climate but also to provide flexibility to adjust flow releases and reduce the gap between drought conditions, which is crucial to allow ecosystem recovery and functioning over time.

It is necessary to shift the perception of system reoperation impacts from a short-term 'crisis response' to a long-term 'risk response.' The findings of this doctoral dissertation demonstrate that considering the long-term effects of operation when designing operating strategies for multiple users leads to improved performance in both hydropower generation and meeting ecosystem demands.

Instead of fixed (static) environmental water needs, implementing dynamic flow regimes (DAE-flows) that combine different flow patterns throughout the planning horizon based on hydrological conditions and long-term functionality enhances the flexibility and resilience of ecosystems. Such an approach conserves water in some periods, at the expense of some environment (e.g., fish recruitment) or hydropower losses, to improve success in the long-term.

Even under a significant dryer climate scenario, a long-term approach to adaptation can allow maintenance and improvement of environmental performance in most years, so during severe droughts the water can still be reallocated to hydropower (as it is currently done) but at a lesser cost to the environment. In this context, water storage becomes increasingly important to meet future energy and environmental needs, given it provides much needed system flexibility.

Reconciling environmental demands and other economic objectives such as hydropower is a water allocation exercise, which bear tradeoffs that need to be evaluated and fairly shared among society who will benefit from both economic outcomes and environmental quality.

By quantifying the tradeoffs across various levels of ecosystem and hydropower performance, it becomes possible to identify points of optimal compromise, facilitating the negotiation process of solutions. Such points indicate that significant environmental restoration can be achieved without overly compromising energy production. Quantifying the trade-offs between ecosystem performance and hydropower objectives facilitates negotiations with electricity and water agencies, enabling a balance between multiple interests.

Finally, successful pathways leading to adaptation to future scenarios when both climate and competing water demands are changing can only be found by constantly exploring new solutions with integrated water and energy policies and mechanisms to avoid the recurring conflict between energy and the environment during droughts. The better the water allocation to ecosystem needs during normal years, the healthier, more resilient it will become, and the better it can withstand incoming droughts and share water with other human demands.